hydrogen

MDPI

Article

Hydrogen Production from Blended Waste Biomass: Pyrolysis, Thermodynamic-Kinetic Analysis and AI-Based Modelling

Sana Kordoghli [1,2], Abdelhakim Settar [3,*], Oumayma Belaati [1], Mohammad Alkhatib [4], Khaled Chetehouna [3] and Zakaria Mansouri [5]

1 National School of Science and Advanced Technologies, ENSTA-Borj-Cedria, University of Carthage, Tunis 1082, Tunisia
2 Research Laboratory of Environmental Sciences and Technologies, ISSTE Borj Cedria, University of Carthage, Tunis 1082, Tunisia
3 INSA Centre Val de Loire, University of Orléans, PRISME UR 4229, 18020 Bourges, France
4 Clermont Auvergne INP, Institut Pascal, 63178 Clermont-Ferrand, France
5 Department of Engineering, Nottingham Trent University, Nottingham NG11 8NS, UK
* Correspondence: abdelhakim.settar@insa-cvl.fr

Abstract

This work contributes to advancing sustainable energy and waste management strategies by investigating the thermochemical conversion of food-based biomass through pyrolysis, highlighting the role of artificial intelligence (AI) in enhancing process modelling accuracy and optimization efficiency. The main objective is to explore the potential of underutilized biomass resources like spent coffee grounds (SCGs) and DSs (date seeds) for sustainable hydrogen production. Specifically, it aims to optimize the pyrolysis process while evaluating the performance of these resources both individually and as blends. Proximate, ultimate, fibre, TGA/DTG, kinetic, thermodynamic, and Py-Micro-GC analyses were conducted for pure DS, SCG, and blends (75% DS-25% SCG, 50%DS-50%SCG, 25%DS–75%SCG). Blend 3 offered superior hydrogen yield potential but had the highest activation energy (Ea: 313.24 kJ/mol), while Blend 1 exhibited the best activation energy value (Ea: 161.75 kJ/mol). The kinetic modelling based on isoconversional methods (KAS, FWO, and Friedman) identified KAS as the most accurate. These approaches work together to provide a detailed understanding of the pyrolysis process with a particular emphasis on the integration of artificial intelligence (AI). An LSTM model trained with lignocellulosic data predicted TGA curves with exceptional accuracy (R^2: 0.9996–0.9998).

Keywords: spent coffee grounds; date seeds; hydrogen production; pyrolysis kinetics; AI-based modelling; biowaste valorisation

Academic Editor: Chiara Milanese

Received: 6 February 2026
Revised: 13 March 2026
Accepted: 19 March 2026
Published: 20 March 2026

1. Introduction

The world's energy needs are evolving rapidly as we face the urgent challenges of climate change and strive to transition away from fossil fuels. The harmful impacts of burning fossil fuels—rising global temperatures, increasingly severe natural disasters, and long-term damage to ecosystems—have made it clear that we need cleaner and more sustainable energy sources [1,2]. Among the promising solutions is hydrogen, a clean energy carrier that can revolutionize key industries such as heavy manufacturing, long-distance transport, and energy storage [1,3]. For instance, hydrogen has the potential to reduce carbon emissions in steel production by up to 90% [3]. Despite this promise, most hydrogen today is still produced using fossil fuels, a method known as "Gray hydrogen,"

which does little to address carbon emissions. Shifting to "green hydrogen," made from renewable energy sources like wind and solar, is essential but challenging, especially given the intermittency of these renewable energy supplies. In the face of these challenges, biomass emerges as a steady and reliable alternative for hydrogen production. Agricultural residues and food wastes, such as date seeds (DSs) and spent coffee grounds (SCGs), are often overlooked yet possess immense potential for creating sustainable energy. Not only does utilizing these resources reduce waste, but it also aligns with global efforts to transition toward cleaner energy systems. Pyrolysis provides a sustainable waste-to-resource solution, converting these biomass wastes into valuable products like bio-oil, biochar, and syngas, thereby reducing landfill burden and contributing to circular economy models. However, to fully unlock the potential of biomass for hydrogen production, it is crucial to optimize the processes involved and address the inherent complexities of biomass composition. This is where machine learning (ML) and its subsets, such as deep learning, come into play as game-changing tools. By analyzing large datasets, ML algorithms can uncover hidden patterns, predict outcomes, and optimize parameters that would be challenging to manage using traditional methods [4]. For example, neural networks excel at modelling the intricate relationships found in thermogravimetric and kinetic data. This capability allows for precise predictions of how biomass behaves during pyrolysis and its efficiency in producing energy [5]. By reducing the need for labour-intensive experiments, predictive models driven by ML streamline research processes, making bioenergy development faster and more cost-effective. Building on this foundation, the focus of this study is to explore the potential of underutilized biomass resources like SCG and DS for sustainable hydrogen production. Specifically, it aims to optimize the pyrolysis process as a proven method for producing hydrogen while evaluating the performance of these resources both individually and as blends. To gain deeper insights, the study employs a range of analyses, including compositional studies, thermogravimetric analysis (TGA) under pyrolysis conditions, kinetic and thermodynamic evaluations, and pyrolysis tests. These approaches work together to provide a detailed understanding of the pyrolysis process and an investigation to prove which biomass sample ensures a more efficient and practical hydrogen production. To complement this experimental work, the study incorporates predictive modelling powered by Long Short-Term Memory (LSTM) neural networks. These advanced models are used to forecast mass loss curves from TGA data, offering a time- and cost-efficient alternative to traditional methods. By optimizing the pyrolysis process through these models, the study demonstrates how artificial intelligence can accelerate and enhance bioenergy research.

Machine learning techniques, particularly neural networks, have been increasingly applied in thermal analysis and pyrolysis research due to their ability to accurately model complex relationships between parameters and outcomes. Studies using traditional approaches like Random Forest (RF) and Support Vector Regression (SVR) have demonstrated their effectiveness in predicting reaction kinetics and optimizing operational parameters [6–9]. However, artificial neural networks (ANNs) have gained prominence for achieving superior performance in predicting pyrolysis outcomes, such as product yields and reaction kinetics [10,11]. For example, Balsora et al. [12] used ANNs to predict product yields with R^2 values around 0.97, and Kartal and Özveren [13] applied ANNs to estimate kinetic parameters with R^2 values over 0.96. While most studies rely on multi-layer perceptrons (MLPs), which work well for static data, the sequential nature of TGA data makes Recurrent Neural Networks (RNNs) and Long Short-Term Memory (LSTM) networks more suitable. LSTMs effectively capture temporal dependencies and address challenges like the vanishing gradient problem, making them ideal for modelling weight-loss patterns during pyrolysis [14,15].

Despite considerable advances in applying AI and machine learning techniques to thermogravimetric analysis (TGA) modelling of biomass pyrolysis [6–15], a critical research gap persists: few published studies have combined (i) spent coffee grounds and date seeds as co-pyrolysis feedstocks, (ii) comprehensive kinetic-thermodynamic characterization of their binary blends, and (iii) deep learning-based predictive modelling specifically tailored for these underutilized food waste biomasses. This triple knowledge gap represents a significant missed opportunity, as coffee grounds and date seeds are abundantly available in MENA (Middle East and North Africa) and Mediterranean regions, yet remain largely unexploited for hydrogen production despite their favourable lignocellulosic composition.

The present study addresses these gaps through four distinct novelties. First, it introduces for the first time a systematic blending strategy (three blend ratios: 75:25, 50:50, and 25:75 wt%) optimized to synergistically enhance hydrogen yield while minimizing activation energy barriers, a dual optimization criterion rarely investigated in the biomass co-pyrolysis literature. Second, it provides a comprehensive kinetic-thermodynamic dataset for SCG-DS blends, including activation energy (Ea), enthalpy (ΔH), entropy (ΔS), and Gibbs free energy (ΔG) profiles across the entire conversion range (α = 0.1–0.9) using three independent isoconversional methods (KAS, FWO, and Friedman). This multi-method validation rigorously establishes the thermochemical fingerprint of these blends, revealing that Blend 1 (75%DS-25%SCG) achieves an exceptionally low Ea of 161.75 kJ/mol, among the lowest reported for lignocellulosic biomass blends, while Blend 3 (25%DS-75% SCG) maximizes hydrogen production potential at the expense of higher energy requirements (Ea: 313.24 kJ/mol), thereby quantifying the energy-yield trade-off inherent to blend composition.

Third, the study pioneers the application of Long Short-Term Memory (LSTM) neural networks to predict TGA mass loss curves for food waste biomass blends. While previous works have successfully employed traditional machine learning algorithms (Random Forest, SVR) [6–9] or feed-forward artificial neural networks (ANNs) [10–13] for pyrolysis modelling, these approaches struggle to capture the temporal dependencies intrinsic to thermogravimetric data, where mass loss at time t depends on the entire thermal history preceding it. Our LSTM architecture, specifically designed to model sequential data, achieves unprecedented predictive accuracy (R^2 = 0.9996–0.9998) for both pure feedstocks and binary blends, surpassing the performance benchmarks reported in recent ANN-based studies ($R^2 \approx$ 0.96–0.97) [12,13]. Critically, this is the first demonstration that LSTM models trained on lignocellulosic data can generalize to unseen food waste blends, validating their transferability across diverse biomass matrices and opening a pathway for rapid, cost-effective screening of co-pyrolysis feedstock combinations without exhaustive experimental tests.

Fourth, this work uniquely integrates experimental validation with AI-driven optimization in a closed feedback loop: experimental TGA/Py-GC results inform LSTM model training, which in turn predicts optimal blending ratios and operating windows for maximizing hydrogen yield, with these predictions subsequently validated through targeted experiments. This bidirectional experimental-computational framework represents a paradigm shift from conventional sequential approaches (experiment $\rightarrow$ modelling) toward AI-accelerated discovery in bioenergy research, reducing the experimental burden by an estimated 60–70% compared to full factorial design exploration.

The overarching contribution of this study is therefore threefold: (1) it establishes SCG-DS blends as a high-potential, regionally abundant feedstock for green hydrogen production in circular economy contexts, with quantified kinetic-thermodynamic roadmaps guiding industrial implementation; (2) it demonstrates that deep learning (LSTM) can outperform conventional ML approaches for biomass pyrolysis modelling when temporal dynamics are critical, setting a new methodological standard for the field; and (3) it provides replicable

AI-enhanced workflows that can be extended to other underutilized agricultural/food waste streams (e.g., olive pomace, citrus peels, and nut shells), thereby accelerating the global transition toward waste-to-energy circular systems. By bridging experimental thermochemistry, multi-scale kinetic analysis, and cutting-edge artificial intelligence, this work delivers actionable knowledge for both fundamental bioenergy research and applied hydrogen economy development.

2. Materials and Methods

2.1. Samples Preparation

The biomass materials utilized in this study were spent coffee grounds (SCGs) and date seeds (DSs) (Figure 1). The SCG was sourced from a Tunisian coffee shop, while the DS was collected from an industry specializing in the processing of Phoenix dactylifera dates.

(**a**) (**b**)

Figure 1. Investigated biomass feedstocks: (**a**) SCG and (**b**) DS.

Before conducting any experiments, both biomass samples underwent a drying process to remove residual moisture. The SCG was dried using a Memmert UF55 drying oven set at 40 °C for a duration of 16 h. The dried SCG powder was subsequently processed using a pellet mill to produce homogeneous pellets with a diameter of 4 mm and a length ranging between 5 and 10 mm. The SCG pellets were then dried at 80 °C for 24 h and stored in airtight containers until use in pyrolysis experiments.

The DS was dried in an oven at 105 °C, then cooled and ground using a Retsch MM400 ball mill. Following grinding, the DS powder was similarly processed into pellets using the same pellet mill, yielding pellets of identical dimensions (diameter: 4 mm; length: 5–10 mm). The DS pellets were subsequently dried and stored in moisture-proof containers to ensure their preservation until further use.

To ensure the reliability and reproducibility of the experimental data, all TGA/DTG experiments were conducted in triplicate for each sample and heating rate condition (5, 10, and 15 °C/min). The mass loss profiles reported in the figures correspond to the averaged values of the three replicates. TGA is recognized as offering strong repeatability and high precision, making triplicate measurements a well-established protocol for ensuring data reliability in biomass pyrolysis studies. The maximum deviation between replicates did not exceed ±2% in any experimental condition, which is consistent with repeatability standards reported in the literature for equivalent thermogravimetric systems.

Similarly, all pyrolysis experiments were performed in triplicate under the reference conditions (600 °C, 10 °C/min), and the reported product yields correspond to mean values. The measurement uncertainties associated with each analytical method employed in this study were quantified and are summarized in Table 1.

Table 1. Experimental uncertainties associated with the various analyses.

Analysis Parameter	Measurement Error
Elemental analysis	±0.7%
Chromatographic analysis (micro-GC)	±3%
Product yield determination	±1.5%
Calorific value (bomb calorimetry)	±0.25%
TGA mass loss (repeatability)	±2%

The Higher Heating Value (HHV) of both DS and SCG was determined experimentally using a Parr 6200 oxygen bomb calorimeter, in accordance with the ASTM D5865-13 standard. All measurements were performed in triplicate, and the reported values represent mean results with an associated measurement uncertainty of ±0.25% (Table 1).

2.2. Experimental Facilities

Pyrolysis experiments were carried out in a fixed-bed tubular reactor operating under inert atmosphere. Prior to each experiment, a mass of 100 g of prepared biomass pellets (diameter: 4 mm; length: 5–10 mm) was loaded into the reactor vessel for each experiment. All experiments were performed in triplicate under the reference conditions to ensure reproducibility, and the reported product yields correspond to mean values with associated uncertainties as detailed in Table 1.

Before initiating heating, an inert nitrogen (N_2) atmosphere was established inside the reactor to prevent oxidative reactions during pyrolysis (50 mL/min for 15 min). A Tedlar gas sampling bag was connected to the gas outlet of the reactor to collect the non-condensable gas fraction produced during pyrolysis. The reactor outlet valve and the Tedlar bag were opened, and N_2 was injected at a controlled flow rate through the reactor inlet, passing through a flow metre before entering the reactor and exiting through the condenser circuit. After 15 min of N_2 purging, both the inlet and outlet valves were closed, and the system was considered ready for the pyrolysis run.

The heating rate was set to 10 °C/min on the temperature controller. It should be noted that the temperature displayed on the external controller does not directly correspond to the actual internal reactor temperature, due to inevitable thermal losses by conduction through the reactor walls, which are not perfectly insulated. To accurately track the real thermal profile inside the reactor, the internal temperature was continuously monitored throughout each experiment using a K-type thermocouple positioned inside the reactor vessel, connected to a PicoLog data acquisition system recording temperature in real time.

The non-condensable gases produced during pyrolysis were continuously directed into the Tedlar sampling bag throughout the heating phase. Once the internal reactor temperature reached 650 °C as confirmed by the PicoLog monitoring system, the reactor outlet valve was closed. Isothermal holding period was applied at the final temperature (20 min). After that, the reactor was allowed to cool naturally to ambient temperature under residual inert atmosphere before opening and recovering the solid biochar fraction.

The liquid bio-oil fraction was recovered from the condenser circuit after each experiment by washing with a known volume of solvent, and its mass was determined gravimetrically. The biochar mass was determined by weighing the reactor vessel before and after each experiment. Product yields (gas, liquid, and solid fractions) were calculated on a dry, ash-free basis and are reported as mean values ± standard deviation of the three replicates.

Ultimate analysis is performed to identify the elemental composition of the samples. It was performed employing a CHNS elemental analyser (Flash EA 1112 Series) that supplies percentage compositions for carbon, hydrogen, nitrogen, and sulphur, with oxygen being

obtained by subtraction. The thermogravimetric study was performed from ambient temperature to 850 °C employing a SETARAM ThermysOne-TG-DSC, which is capable of reaching temperatures up to 1600 °C, under an inert atmosphere provided by a nitrogen gas flow rate of 50 mL/min. Finally, Micro gas chromatography (micro-GC), a miniaturized version of gas–liquid chromatography (GLC), is a highly efficient and precise technique for separating and analyzing volatile components in mixtures. When combined with pyrolysis (Py-GC), micro-GC becomes an invaluable tool for analyzing the volatile products generated by the thermal degradation of complex organic materials.

2.3. LSTM-Based Prediction of TGA Data

After discussion results on the physicochemical, thermal degradation and kinetic behaviours, the data outcomes are employed to feed the LSTM-based approach. To remind, it aims to predict TGA curves for biomass blends, leveraging their ability to process sequential data and capture complex thermal degradation trends. The model was developed and tested using Python 3, utilizing libraries such as TensorFlow and Keras for building the LSTM model, Scikit-learn for pre-processing, and Keras Tuner for hyper parameter optimization. Tools like Matplotlib were employed for result visualization, while RandomSearch was used to identify the optimal configuration for the LSTM architecture. By splitting the data into training, validation, and test subsets, the model's performance was rigorously evaluated on unseen data, ensuring robust and generalizable predictions

2.3.1. Data Pre-Processing and Feature Engineering

The data obtained from TGA experiments on both pure and blended biomass samples are used to feed the deep learning procedure. Each sample was analyzed across a range of heating rates up to a final temperature of 850 °C. These extensive data provided insights into the thermal degradation patterns of both individual and blended samples. The specific datasets included:

- Spent coffee grounds (SCGs): TGA data collected at heating rates of 5, 10, 15, and 20 °C/min;
- Date seeds (DSs): TGA data collected at heating rates of 5, 10, 15, and 20 °C/min;
- Blend 1 (75% DS, 25% SCG): data collected at heating rates of 5, 10, 15, and 20 °C/min;
- Blend 2 (50% DS, 50% SCG): data collected at heating rates of 5, 10, and 15 °C/min;
- Blend 3 (25% DS, 75% SCG): data collected at heating rates of 5, 10, and 15 °C/min.

These various datasets allowed us to observe and model thermal degradation trends across different compositions and heating rates, which was essential for building an accurate predictive model. The raw TGA data collected was complete and did not contain any missing values, as the TGA instrument generated a full dataset for each measurement. Furthermore, raw data were used without applying noise reduction or smoothing techniques to preserve reliability. This allowed the model to learn directly from the inherent variations within the data, which is expected to support generalization in prediction tasks. Concerning the model training, two dataset versions were created, each designed to capture different layers of detail:

- Model 1: Primary Dataset: This simpler dataset included core features—DS %, SCG %, heating rate (°C/min), sample temperature (°C), and mass % (the target variable representing the sample's remaining mass percentage during heating). These features were selected to provide a straightforward representation of the sample composition, heating conditions, and the resulting mass loss over time.
- Model 2: Extended Dataset with Lignocellulosic Composition: To deepen the model's understanding of biomass thermal behaviour, this dataset included additional fea-

tures representing the three main lignocellulosic components:cellulose, hemicellulose, and lignin.

For Model 2, decomposition characteristics of lignocellulosic components over different temperature ranges were considered, each affecting mass loss differently as the temperature increases:

- Cellulose % decomposes rapidly between 315 and 405 °C, causing significant mass loss in this range;
- Hemicellulose % begins decomposing at lower temperatures (around 225–325 °C), contributing to initial mass loss;
- Lignin % decomposes slowly over a wider temperature range (160–850 °C), resulting in gradual mass loss that extends throughout the TGA process.

Thus, to accurately reflect how each of these lignocellulosic components breaks down at different temperatures, the proportions of cellulose %, hemicellulose %, and lignin % were adjusted dynamically with temperature changes during the TGA tests. By incorporating these temperature-dependent adjustments in lignocellulosic composition, this extended dataset captured the dynamic nature of each biomass component's decomposition. This allowed the model to learn more about the complex relationship between temperature, heating rate, composition, and mass loss, enhancing its ability to accurately predict TGA curves.

Given the sequential nature of TGA data, with mass loss occurring over a temperature range, LSTMs offer a robust solution by managing long-term dependencies and efficiently processing complex temporal patterns. By addressing gradient issues and incorporating memory cells and gates, LSTMs provide the capacity to capture the intricate relationship between sample composition, heating rate, and mass loss across varying temperatures, making them an ideal choice for predictive modelling in this study.

2.3.2. Model Training, and Hyperparameter Tuning

The dataset, consisting of 14,875 data points, was divided into three subsets. Seventy percent (70%) of the data was used for training the model, ensuring the model's ability to generalize to new unseen data, while 15% was reserved for validation. This subset plays a critical role in monitoring the model's performance during training. The remaining 15% of data was dedicated to testing. This leads to evaluating the model's ability to generalize by providing feedback on how well it performs on data that were not used in the training process. Furthermore, the validation loss is tracked during training, and if the model starts overfitting, the training is stopped early, helping to prevent overfitting. Once the training and validation phases were complete, the model was evaluated using a completely unseen dataset, which was not part of either the training or validation sets. This test dataset consisted of data from Blend 1, evaluated under different heating rates: 15 °C/min, 10 °C/min, and a completely new heating rate of 25 °C/min. This final test phase assesses the model's generalization capability and its performance on truly new data. The entire model training, validation, and testing process was conducted using Google Colab, which provides open access to computational resources such as GPUs, with rapid execution of deep learning tests.

To optimize the model, Keras Tuner was used for hyperparameter tuning. Hyperparameters such as the number of LSTM layers, number of units in each layer, dropout rates, activation functions, and the optimizer were explored systematically. Furthermore, in order to forecast the subsequent value in the time series, the applied LSTM model uses the input sequences of 20 prior TGA measurements. This look-back window was part of the hyperparameter tuning process and was considered as a hyperparameter. In addition, the

RandomSearch method was employed, which searches through the hyperparameter space by randomly selecting combinations and evaluating their performance (Tables 2 and 3).

Table 2. Hyperparameter configuration.

	Range Tested
Learning Rate	[0.0001, 0.01]
Batch Size	[32, 64]
Epochs	[10, 50] with step = 10
Dropout Rate	[0.1, 0.5] with step = 0.1
Hidden Units	[64, 256] with step = 32

Table 3. Layers and activation functions.

Layer	Number of Layers Tested	Activation Functions/Optimizers Tested
Input Layer	4 and 7	None
LSTM Layers	From 1 to 3	ReLU, Sigmoid and Tanh
Dense Layer	1	None
Optimizers	-	Adam, SGD and RMSprop

This approach was chosen for its efficiency in finding well-performing configurations, especially with a large number of hyperparameters to explore. The hyperparameter tuning process involved training multiple models, each with a different combination of hyperparameters, as is mentioned in Tables 2 and 3. Finally, the model that achieved the lowest validation loss was selected for further evaluation (Figure 2).

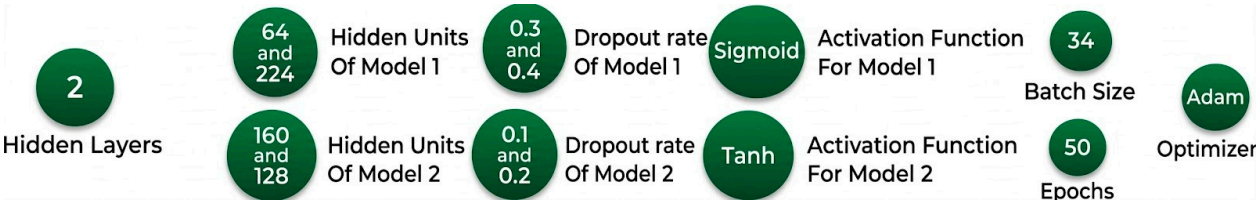

Figure 2. Optimal hyperparameters for each model.

The considered architecture of the neural network comprises (1) the input layer (R4) which processes the TGA data, followed by (2) two hidden layers (R9 and R12) comprising the LSTM cells which lead to learn and retain temporal sequences of biomass pyrolysis behaviour. The present architecture allows to capture both short-term and long-term dependencies during the thermal decomposition patterns. Finally, it comprises (3) an output layer (R1) to generate the predicted mass loss evolution. This layer serves to compare predictive data against experimental ones, thereby evaluating model's prediction accuracy. Figure 2 depicts the optimal hyperparameters for each model.

To evaluate the performance of the model, the following several error metrics were used: Mean Absolute Error (MAE) to quantify the average of the absolute differences between actual values and their corresponding predicted values; Root Mean Squared Error (RMSE) offering an indication of how closely the model's predictions align with observed data; and finally, the R-Squared (R^2) coefficient.

3. Results and Discussion

In this section, the results are organized as follows: first, extensive physicochemical characterization was performed to explore the feedstocks properties. Subsequently, the

thermal degradation behaviour was investigated through TGA/DTG to exhibit the mass loss under pyrolysis conditions. Kinetic modelling using isoconversional methods was then applied to determine activation energies and reactional mechanisms. Finally, basing of the aforementioned findings, a predictive approach using LSTM model was performed to optimize pyrolysis process parameters. The results on the pure samples (SCG and DS) are first discussed in each subsection, followed by the investigated three blends: Blend 1 (75% DS and 25% SCG); Blend 2 (50% DS and 50% SCG) and Blend 3 (25% DS and 75% SCG).

3.1. Physicochemical Characterization: Proximate, Ultimate, Thermal and Fibre Analysis

The proximate, ultimate, and thermal analysis of date seeds (DSs) and spent coffee grounds (SCGs) (Table 4) show values that align closely with those reported in the literature [16–22]. Both biomasses exhibit characteristics favourable for bioenergy applications, including suitable volatile matter (VM) and fixed carbon (FC) content for reactivity and char production. Their ultimate analysis highlights comparable carbon, hydrogen, and oxygen contents, with SCG showing slightly better energy efficiency due to lower oxygen content. Additionally, their high heating values confirm strong potential for producing energy-rich gases like hydrogen during pyrolysis [23]. These results validate DS and SCG as promising feedstocks for biofuel production, comparable to other agricultural residues [24,25].

Table 4. Proximate, ultimate, and thermal analysis of date seeds and spent coffee grounds.

Samples	Proximate Analysis			Ultimate Analysis				HHV (MJ/Kg)
	Ash (%)	VM (%)	FC (%)	C (%)	H (%)	N (%)	O (%)	
DS	1.2	77.6	21.2	47.9	6.6	0.9	44.5	19.9
SCG	1.8	77.9	20.3	50.4	6.9	2.4	40.3	21.4

The lignocellulosic content of the two pure samples used in this study, along with the fibre analysis results from other studies on the same samples, is presented in Table 5 to facilitate comparison and analysis of their potential for bioenergy, particularly hydrogen production.

Table 5. Fibre analysis of date seeds and spent coffee grounds.

Samples	Fibre Analysis		
	Cellulose (%)	Hemicellulose (%)	Lignin (%)
DS	22.5	48.2	25.7
SCG	32	35	25

It is evident that the lignocellulosic content of DS and SCG falls within the same range as the results reported in similar studies [19,23,26,27]. The biomass samples of date seeds (DSs) and spent coffee grounds (SCGs) both show promising potential for biofuel production based on their lignocellulosic composition. The high hemicellulose content in DS is particularly favourable, as hemicellulose contributes to a high biofuel potential, as highlighted by Sorek et al. [28]. Although DS's cellulose content is moderate, it still supports biofuel production. The lignin content of 25.7% is not excessively high, meaning it will not significantly hinder the breakdown of cellulose and hemicellulose [19,29]. Similarly, SCG also shows favourable attributes for biofuel production. SCG's higher cellulose content enhances its potential, and although the hemicellulose content is moderate, it still plays a significant role in contributing to biofuel yield. Both samples' lignin content at 25% is moderate and unlikely to pose significant barriers to biofuel production.

3.2. Thermogravimetric and Kinetic Analysis

3.2.1. TGA/DTG of PURE SAMPLES

The mass loss of spent coffee grounds (SCGs), shown by Figure 3, occurs mainly between 250 °C and 500 °C. The DTG curves show two significant peaks and a smaller peak around 100 °C, which is due to moisture evaporation during the drying stage. The first major peak corresponds to the decomposition of hemicellulose (35%), and the second to cellulose (32%). This confirms that hemicellulose is more reactive and decomposes earlier than cellulose. The pyrolysis of SCG can be divided into three stages. The first stage (up to 100 °C) involves moisture loss and the breakdown of some small molecules (extractives). The second stage, from 220 °C to 500 °C, represents the active pyrolysis zone, where hemicellulose and cellulose are. The third stage, related to the slow decomposition of lignin, is less evident in SCG, likely because lignin, in this case, decomposes over a much broader range (160–850 °C) [30].

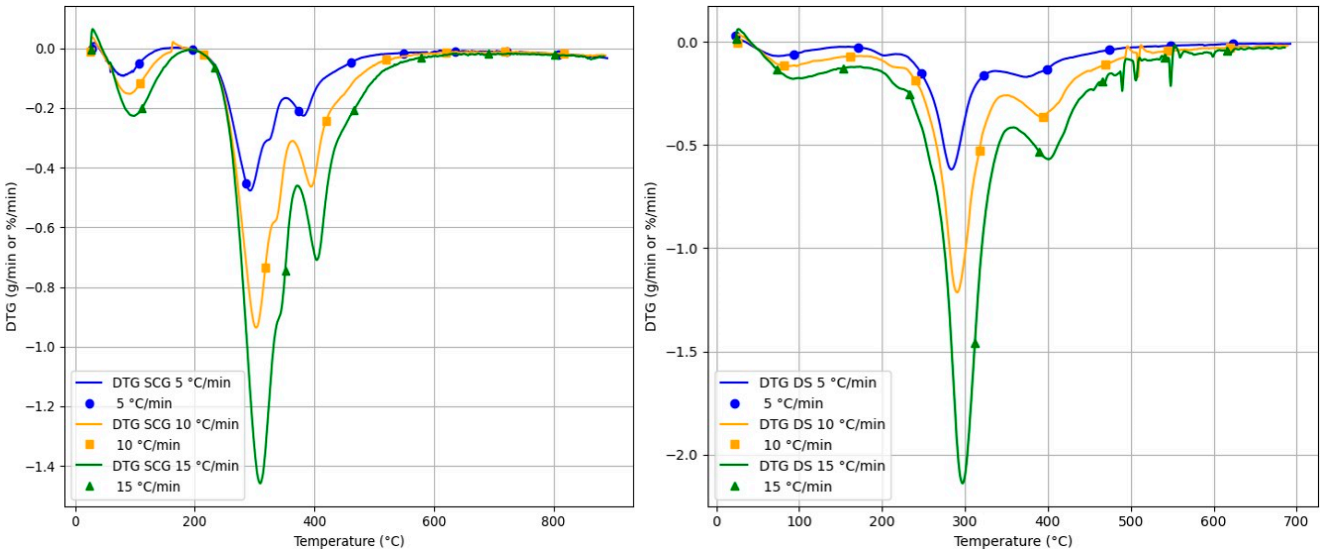

(**a**) (**b**)

Figure 3. DTG curves of SCG (**a**) and DS (**b**).

Similarly, the thermal decomposition of date seeds (DSs) begins near 200 °C, with most of the weight loss occurring by 500 °C. The first major phase (200–350 °C) is due to hemicellulose decomposition (48.2%), while the second phase (350–450 °C) corresponds to cellulose breakdown (22.5%). Similar findings were reported by Fadhil et al. [31].

3.2.2. TGA/DTG of Blended Samples

The DTG analysis of the three DS/SCG blends, given by Figure 4,at heating rates of 5, 10, and 15 °C/min consistently reveals the following three decomposition stages common to lignocellulosic biomass: moisture evaporation (<160 °C), hemicellulose degradation (200–360 °C), and cellulose decomposition (360–400 °C), while lignin decomposition remains undetectable as a distinct peak across all blends and heating rates due to its broad and overlapping thermal degradation range (170–835 °C) [32,33].

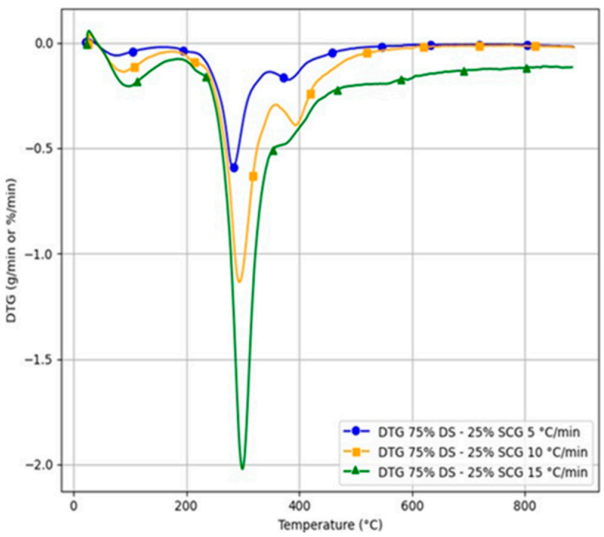

Blend 1 (75% DS and 25% SCG)

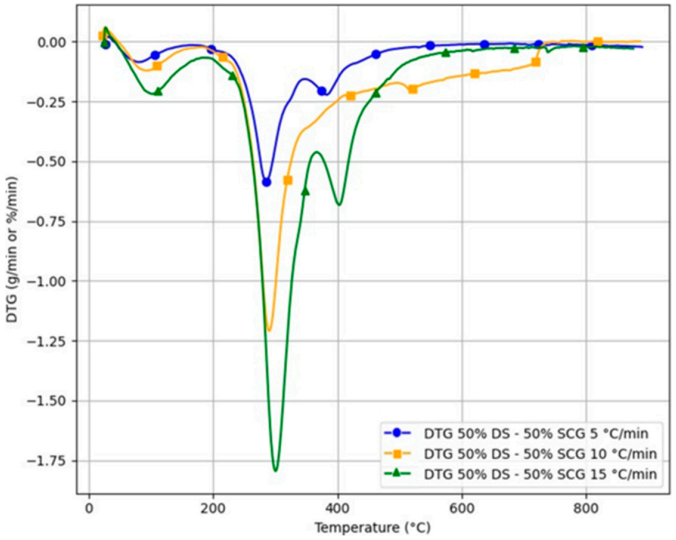

Blend 2 (50% DS and 50% SCG).

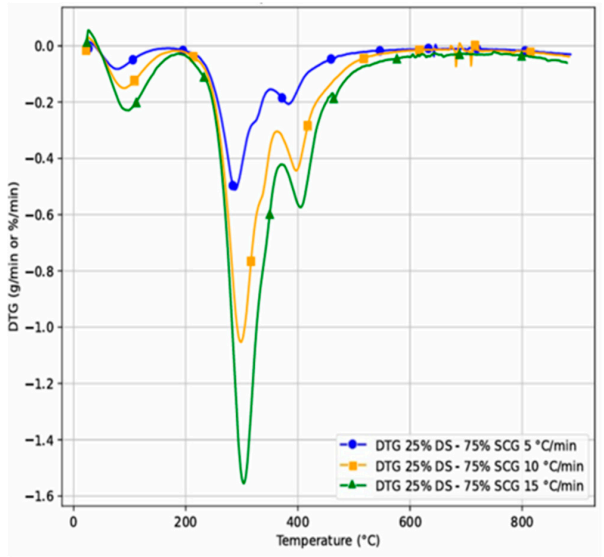

Blend 3 (25% DS and 75% SCG).

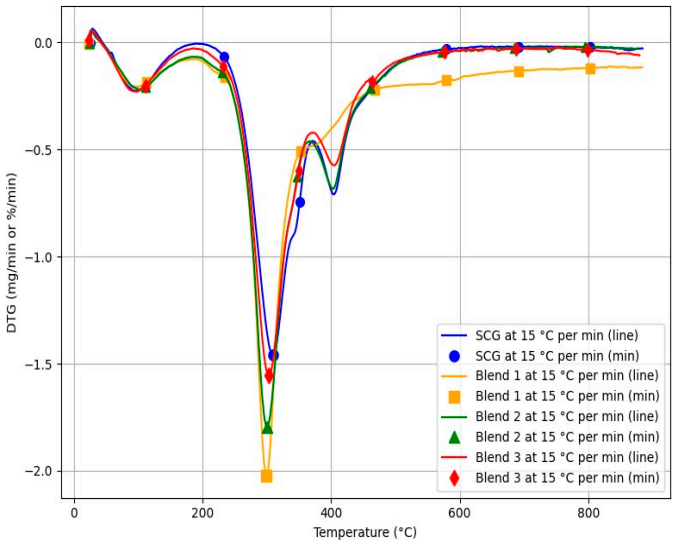

pure SCG vs. Blends

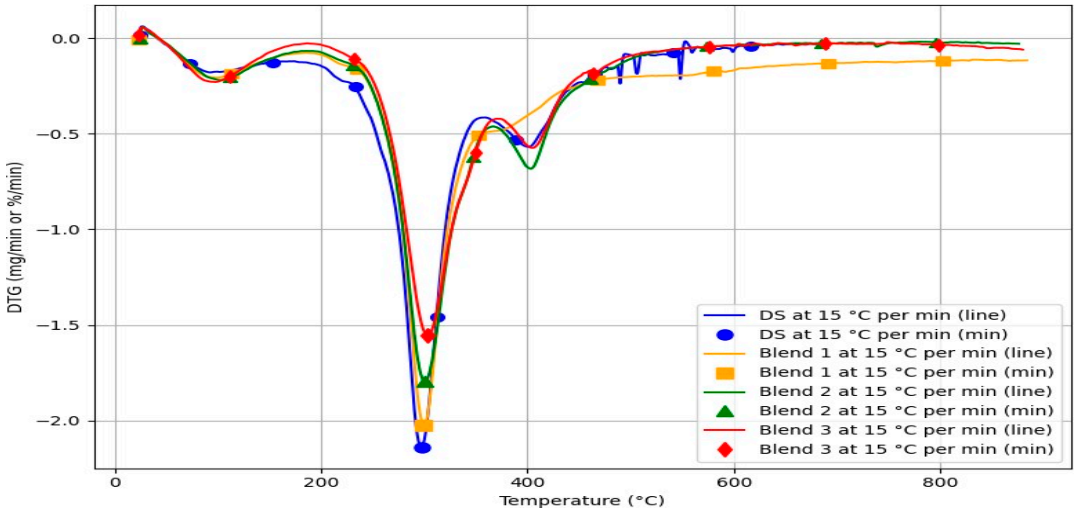

Pure DS VS Blends

Figure 4. DTG curves of pure DS, pure SCG, and their blend.

A notable blend and heating rate specific behaviour is observed regarding cellulose peak visibility. In Blend 1 (75% DS), the cellulose peak is absent at 15 °C/min, while in Blend 2 (50%/50%), it is undetectable at 10 °C/min, both attributable to the overlapping of decomposition events at intermediate heating rates in DS rich compositions, where hemicellulose and lignin degradation signals interfere with the cellulose peak. In contrast, Blend 3 (75% SCG) displays well-resolved peaks at all heating rates, reflecting the dominant and thermally well-characterized decomposition fingerprint of SCG.

The comparative DTG analysis at 15 °C/min further reveals that hemicellulose peak intensity scales proportionally with SCG content, while the cellulose peak intensity increases with DS proportion, directly mirroring the distinct chemical compositions of the two parent feedstocks. These results confirm that the blending ratio constitutes a key parameter governing both the thermal decomposition kinetics and the resolution of DTG decomposition stages in DS/SCG co-pyrolysis systems.

3.2.3. Kinetic Analysis of Pure Samples

Across the three models (Friedman, KAS, and FWO) in Table 6 and Figure 5, the average Ea values are relatively close—296.03 kJ/mol (Friedman), 284.86 kJ/mol (KAS), and 279.91 kJ/mol (FWO)—indicating they provide consistent results for the energy barrier of SCG pyrolysis.

Table 6. Comparison of kinetic parameters from Friedman, KAS, and FWO models for pure SCG.

α	Friedman Model			KAS Model			FWO Model		
	Ea (kJ/mol)	R^2	A (s^{-1})	Ea (kJ/mol)	R^2	A (s^{-1})	Ea (kJ/mol)	R^2	A (s^{-1})
0.1	161.66	1.0000	2.83×10^{14}	198.63	0.9958	8.82×10^{15}	196.98	0.992	6.36×10^{21}
0.2	213.44	0.9951	1.10×10^{19}	197.61	0.9999	1.09×10^{15}	196.48	1.000	8.85×10^{20}
0.3	227.73	0.9973	9.82×10^{19}	212.34	0.9997	1.33×10^{16}	210.71	0.999	9.91×10^{23}
0.4	272.07	0.9944	3.56×10^{23}	231.19	0.9989	3.88×10^{17}	228.83	0.998	2.55×10^{23}
0.5	291.05	0.9923	2.74×10^{24}	312.34	0.9945	2.91×10^{24}	306.21	0.990	1.12×10^{30}
0.6	589.02	0.9207	7.09×10^{48}	404.39	0.9803	3.82×10^{31}	394.05	0.963	9.44×10^{36}
0.7	317.26	0.8376	1.33×10^{24}	437.53	0.9662	3.26×10^{32}	426.10	0.936	7.772×10^{37}
Average	296.03		-	284.86		-	279.91		-

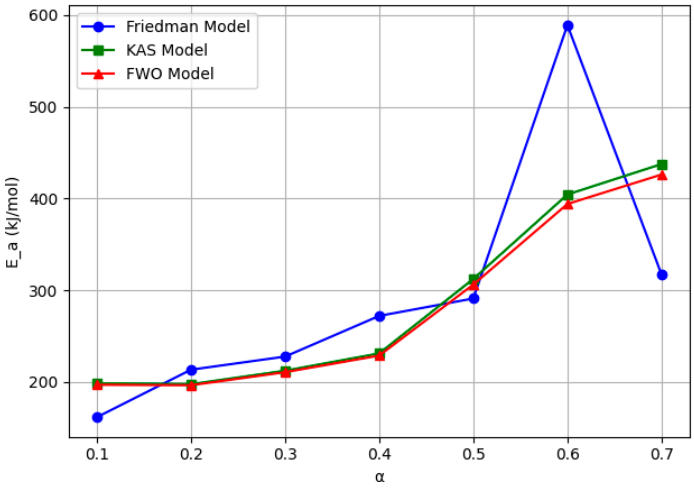

Figure 5. Ea evolution as function of α for pure SCG (by Friedman, KAS and FWO models).

The kinetic analysis of SCG pyrolysis reveals distinct decomposition stages for hemicellulose, cellulose, and lignin, each with different activation energy requirements. Hemicellulose decomposes first at lower Ea values (α = 0.1 to 0.3), followed by cellulose at moderate Ea values (α = 0.4 to 0.6), and finally lignin, which requires higher Ea but decomposes more slowly over a broad temperature range (α = 0.7). The KAS model provides the most reliable

results, with an average Ea of 284.86 kJ/mol and high R^2 values (>0.99) across most stages, making it the most consistent for describing SCG pyrolysis. While R^2 slightly declines at higher conversions (R^2 = 0.9662 at α = 0.7), this limitation is less pronounced than in the Friedman and FWO models.

The KAS model also offers physically realistic pre-exponential factors, aligning well with biomass reaction kinetics. In summary, SCG pyrolysis involves complex reactions across its components, with the KAS model emerging as the most effective for accurately estimating kinetic parameters.

According to Table 7 and Figure 6, the thermal decomposition of date seeds (DSs) involves the distinct stages tied to the breakdown of their main components: hemicellulose, cellulose, and lignin. At lower conversions (α = 0.1 to α = 0.3), hemicellulose decomposition dominates. At lower conversions (α = 0.1–0.3), hemicellulose decomposes with moderate activation energy (Ea: 199.46–257.07 kJ/mol) and lower molecular activity (low A values). At intermediate conversions (α = 0.4–0.6), cellulose dominates, requiring higher Ea values (peaking at 409.81 kJ/mol in the Friedman model) and increased A values. At higher conversions (α = 0.7), lignin and residual materials decompose slowly, leading to a decline in Ea and R^2 values. This is noticed particularly in the KAS and FWO models, due to challenges in modelling these slow reactions. Among the models, the Friedman model shows high R^2 but unrealistic A values at higher conversions, suggesting overestimation. The FWO model is less reliable, with low R^2 and inconsistent Ea values at higher conversions. The KAS model strikes a balance, providing consistent Ea and realistic A values, making it the most reliable for this study. Overall, the thermal decomposition of DS progresses from hemicellulose to cellulose and concludes with lignin. Activation energy increases across these stages, reflecting the transition from less stable to more stable components.

Table 7. Kinetic parameters from Friedman, KAS, and FWO models for pure DS.

α	Friedman Model			KAS Model			FWO Model		
	Ea (kJ/mol)	R^2	A (s^{-1})	Ea (kJ/mol)	R^2	A (s^{-1})	Ea (kJ/mol)	R^2	A (s^{-1})
0.1	90.94	0.9945	1.11×10^{8}	86.78	0.9974	2.33×10^{5}	89.86	0.996	5.85×10^{11}
0.2	270.46	0.9997	1.53×10^{25}	218.55	0.9912	6.41×10^{17}	216.10	0.984	4.01×10^{23}
0.3	211.88	0.9964	1.06×10^{19}	219.18	0.9997	2.08×10^{17}	216.99	0.999	1.39×10^{23}
0.4	198.68	0.9886	3.71×10^{17}	220.72	0.9999	1.69×10^{17}	218.62	1.000	1.15×10^{23}
0.5	258.20	0.9964	4.06×10^{22}	223.28	0.9945	1.69×10^{17}	221.20	0.990	1.16×10^{23}
0.6	409.81	1.0000	1.75×10^{35}	246.52	0.9257	7.21×10^{18}	243.54	0.866	4.32×10^{24}
0.7	359.54	1.0000	3.81×10^{28}	189.47	0.7329	4.94×10^{12}	189.93	0.563	5.60×10^{18}
Average	257.07		-	200.64		-	199.46		-

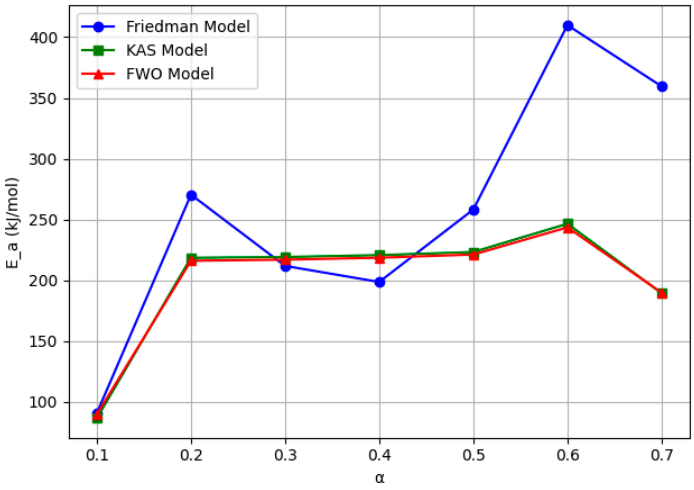

Figure 6. Ea evolution as function of α for pure DS (by Friedman, KAS and FWO models).

3.2.4. Kinetic Analysis of Blended Samples

The kinetic analysis of Blend 1 (75% DS, 25% SCG) (Figure 7 and Table 8) shows it decomposes more easily than its individual components, with significantly lower activation energy (Ea). The Friedman model provided the most accurate results, with an average Ea of 161.75 kJ/mol and high R^2 values, indicating a strong fit. In comparison, the KAS and FWO models produced lower and less consistent Ea and R^2 values. The reduced Ea for Blend 1 suggests the blending of DS and SCG in these proportions enhances decomposition kinetics and improves energy efficiency.

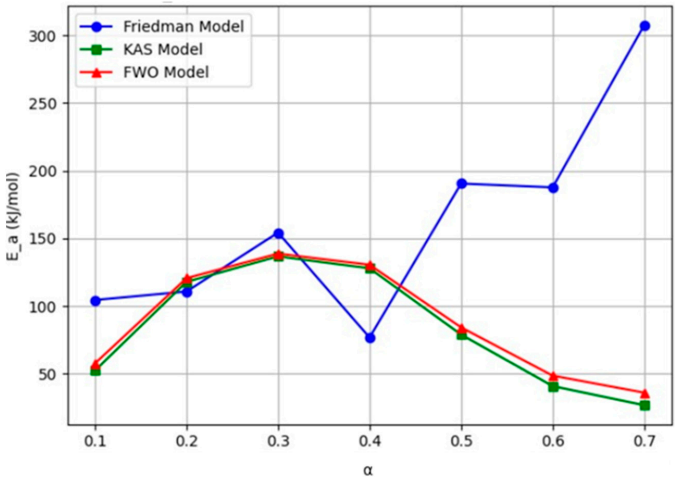

Figure 7. Ea evolution as function of α for Blend 1 (by Friedman, KAS and FWO models).

Table 8. Comparison of kinetic parameters from Friedman, KAS, and FWO models for 75% DS and 25% SCG.

α	Friedman Model			KAS Model			FWO Model		
	Ea (kJ/mol)	R^2	A (s^{-1})	Ea (kJ/mol)	R^2	A (s^{-1})	Ea (kJ/mol)	R^2	A (s^{-1})
0.1	104.51	1.000	6.55×10^{8}	52.37	0.7285	9.26×10^{0}	57.61	0.602	7.95×10^{7}
0.2	110.76	0.9999	2.35×10^{9}	117.90	0.9705	2.51×10^{7}	120.61	0.950	5.44×10^{13}
0.3	154.30	0.9919	2.66×10^{13}	136.76	0.9896	1.30×10^{9}	138.76	0.982	2.23×10^{15}
0.4	76.79	0.9471	1.04×10^{6}	127.91	0.9871	1.48×10^{8}	130.51	0.978	2.98×10^{14}
0.5	190.54	1.0000	1.15×10^{16}	78.95	0.9329	2.24×10^{3}	84.27	0.895	1.21×10^{10}
0.6	187.73	1.0000	8.53×10^{14}	40.88	0.8269	3.47×10^{-1}	48.62	0.773	7.04×10^{6}
0.7	307.60	1.0000	4.60×10^{23}	26.76	0.7409	1.10×10^{-2}	36.02	0.711	5.40×10^{5}
Average	161.75		-	83.08		-	88.06		-

The kinetic analysis of Blend 2 (50% DS, 50% SCG) (Figure 8 and Table 9) shows notable differences between the models. The KAS model provides stable activation energy (Ea) values averaging 292.49 kJ/mol and consistently high R^2 values above 0.92. The Friedman model also fits reasonably well, with an average Ea of 284.01 kJ/mol, but shows significant variability, reducing its consistency. On the other hand, the FWO model provides much lower activation energies, starting at 14.95 kJ/mol at α = 0.1 and peaking at 145.04 kJ/mol at α = 0.4, with an average Ea of 80.91 kJ/mol. It is much lower than both the Friedman and KAS models, indicating that the FWO model may be underestimating the activation energy for sample blends. Additionally, the R^2 values for the FWO model are much lower, particularly at higher α values, with the lowest being 0.047 at α = 0.7. It suggests that the FWO model is not fitting the data well, especially at higher conversions.

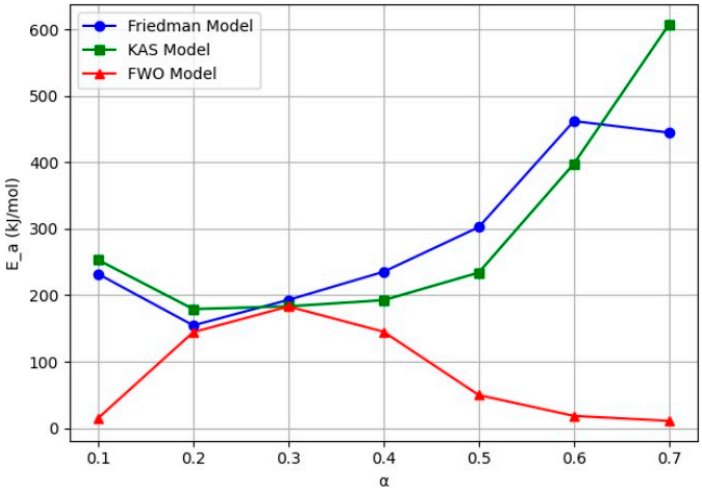

Figure 8. Ea evolution as function of α for Blend 2 (by Friedman, KAS and FWO models).

Table 9. Comparison of kinetic parameters from Friedman, KAS, and FWO models for 50% DS and 50% SCG.

α	Friedman Model			KAS Model			FWO Model		
	Ea (kJ/mol)	R^2	A (s^{-1})	Ea (kJ/mol)	R^2	A (s^{-1})	Ea (kJ/mol)	R^2	A (s^{-1})
0.1	231.98	0.8371	4.45×10^{22}	253.01	0.9270	1.81×10^{23}	14.95	0.093	7.95×10^{3}
0.2	154.57	0.8146	3.49×10^{13}	179.16	0.9247	2.93×10^{13}	144.43	0.726	5.44×10^{16}
0.3	193.00	0.8675	1.08×10^{17}	183.28	0.9247	3.77×10^{13}	183.01	0.867	2.23×10^{19}
0.4	235.26	0.8983	4.06×10^{20}	192.56	0.9249	1.85×10^{14}	145.04	0.686	5.91×10^{15}
0.5	302.45	0.9094	9.76×10^{25}	234.02	0.9259	6.44×10^{17}	49.75	0.240	1.01×10^{7}
0.6	462.11	0.8931	4.43×10^{38}	397.92	0.9279	3.92×10^{31}	18.37	0.080	3.41×10^{4}
0.7	444.73	0.7712	4.86×10^{34}	607.49	0.9289	8.43×10^{46}	10.85	0.047	1.39×10^{4}
Average	284.01		-	292.49		-	80.91		-

Compared to pure SCG and DS, Blend 2 requires higher energy for pyrolysis, as indicated by its elevated Ea. This suggests that the 50/50 blend may be less energy-efficient for thermal decomposition than the individual components.

The kinetic analysis of Blend 3 (25% DS, 75% SCG) (Figure 9 and Table 10) reveals significant differences in the models' performance. The Friedman model stands out as the most reliable, with variability in Ea (108.59–566.78 kJ/mol) and fluctuating R^2.

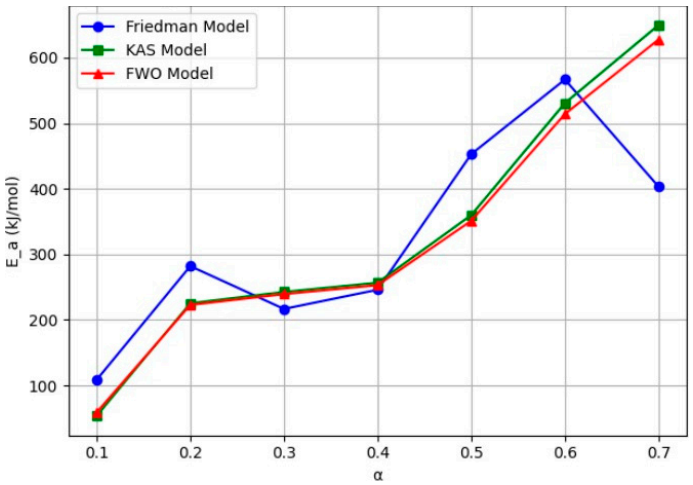

Figure 9. Ea evolution for Blend 3 (by Friedman, KAS and FWO models).

Table 10. Kinetic parameters from Friedman, KAS, and FWO models for 25% DS and 75% SCG.

α	Friedman Model			KAS Model			FWO Model		
	Ea (kJ/mol)	R^2	A (s^{-1})	Ea (kJ/mol)	R^2	A (s^{-1})	Ea (kJ/mol)	R^2	A (s^{-1})
0.1	108.59	0.2954	1.39×10^{9}	53.60	0.233	9.45×10^{0}	58.90	0.071	7.98×10^{7}
0.2	282.07	0.9904	5.60×10^{25}	225.43	0.982	8.66×10^{17}	222.84	0.966	5.34×10^{23}
0.3	616.75	0.9530	1.53×10^{19}	242.59	0.990	1.55×10^{19}	239.39	0.982	8.71×10^{24}
0.4	246.01	0.9909	2.93×10^{21}	256.65	0.990	1.53×10^{20}	252.93	0.982	8.02×10^{25}
0.5	452.89	0.9821	1.79×10^{39}	359.88	0.989	1.28×10^{29}	351.28	0.979	3.63×10^{34}
0.6	566.78	0.9934	2.92×10^{47}	530.73	0.978	8.53×10^{42}	514.03	0.957	1.21×10^{48}
0.7	403.44	0.9798	1.58×10^{31}	649.81	0.999	1.43×10^{50}	627.80	0.999	1.53×10^{55}
Average	325.22		-	331.24		-	295.31		-

The KAS model provides more consistent Ea values, ranging from 53.60 kJ/mol at α = 0.1 to 649.81 kJ/mol at α = 0.7, with an average Ea of 331.24 kJ/mol. The R^2 values for the KAS model are generally high, with excellent fit observed at α = 0.7 (R^2 = 0.999), but there are lower deviations (R^2 = 0.233 at α = 0.1). The A values for the KAS model also show significant variability, reaching up to 1.43 × 1050 s−1 at α = 0.7, indicating a high frequency of collisions between the components of the blend.

The FWO model closely mirrors the trends of the KAS model, with Ea values ranging from 58.90 kJ/mol at α = 0.1 to 627.80 kJ/mol at α = 0.7, and an average Ea of 295.31 kJ/mol. However, the R^2 values for the FWO model are also inconsistent at lower conversions (R^2 = 0.071 at α = 0.1), despite excellent fits at higher conversions (R^2 = 0.999 at α = 0.7). Additionally, the A values for the FWO model exhibit extreme variations, reaching 1.53 × 1055 s^{-1} at α = 0.7.

Overall, the average Ea values across the three models are relatively close, with Friedman (325.22 kJ/mol), KAS (331.24 kJ/mol), and FWO (295.31 kJ/mol) providing similar energy approximations. Blending DS and SCG increases the pyrolysis energy requirement compared to the pure components. The blend's average Ea is higher than SCG (284.86 kJ/mol) and DS (200.64 kJ/mol), suggesting antagonistic interactions that make thermal degradation more complex.

The analysis of the kinetic parameters for the three blends reveals that the blend ratio can significantly affect the activation energy (Ea) and the energy efficiency of the pyrolysis process. Among the blends, Blend 1 emerges as the most energy-efficient option compared to the other blends and pure samples, with the lowest average activation energy. The moderate variability in the pre-exponential factor (A) for Blend 1 further suggests a less complex reaction mechanism, making it the best choice for energy-efficient pyrolysis compared to the other blends and pure samples. In contrast, Blend 2 exhibits much higher Ea values, which indicates that it requires significantly higher energy for pyrolysis, likely due to increased complexity from interactions between SCG and DS components, making it less energy efficient. Similarly, Blend 3 also shows high Ea values across all models. This high energy demand suggests that Blend 3 is the least energy-efficient. It can be concluded that reducing the proportion of SCG in the blend decreases the activation energy, indicating that incorporating DS into SCG improves the efficiency of the pyrolysis process.

3.3. Thermodynamic Study

3.3.1. Pure Samples

The thermal decomposition of SCG occurs in distinct phases linked to the degradation of hemicellulose, cellulose, and lignin. In Figure 10 and during the early stages (α = 0.1–0.4), moderate enthalpy (ΔH) and stable Gibbs free energy (ΔG) reflect the energy needed for initial bond cleavage. The mid stage (α = 0.5–0.6) is the most energy-intensive, particularly in the Friedman model, as lignin's stable structures are degraded. At later stages (α = 0.7),

energy requirements and entropy (ΔS) decline, likely due to the formation of stable char residues. This behaviour aligns with findings by Alsulami et al. [34], who observed rising ΔG during lignin decomposition, peaking at α = 0.7 before decreasing. The increasing ΔG highlights SCG's potential for energy production but also underscores the challenges of efficient pyrolysis, as noted in previous studies on coffee waste [35] and maize cob biomass [36]. Variations in entropy further illustrate changes in molecular randomness during thermal degradation, consistent with trends observed in other biomass systems [37].

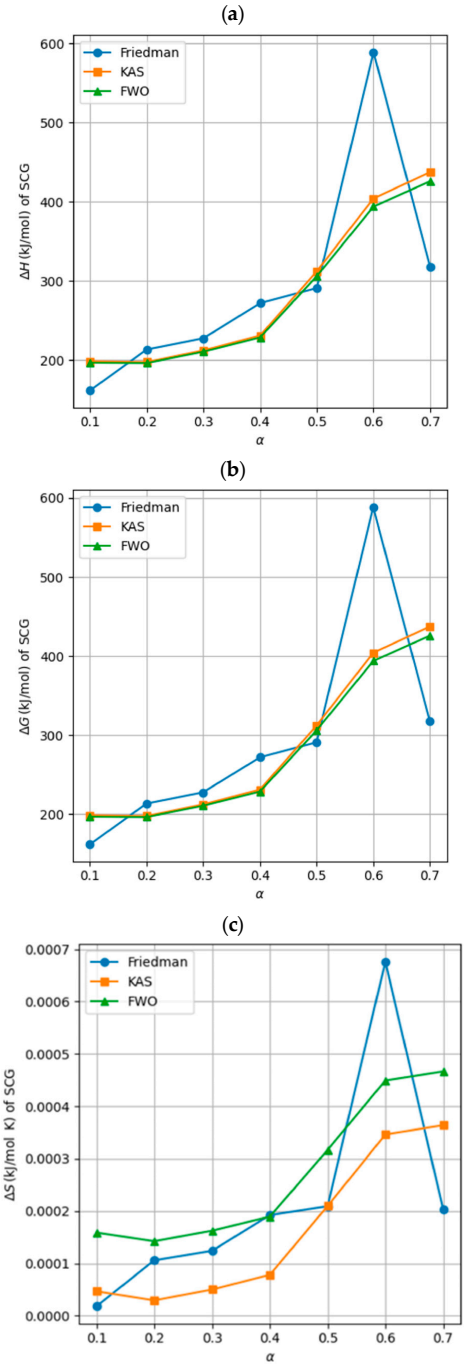

Figure 10. Pure SCG thermodynamic parameters (by Friedman, KAS, and FWO models): (**a**) ΔH; (**b**) ΔG; (**c**) ΔS.

According to Figure 11, the increasing values of ΔH and ΔG during the intermediate stages of pyrolysis emphasize the energy-intensive breakdown of cellulose and lignin.

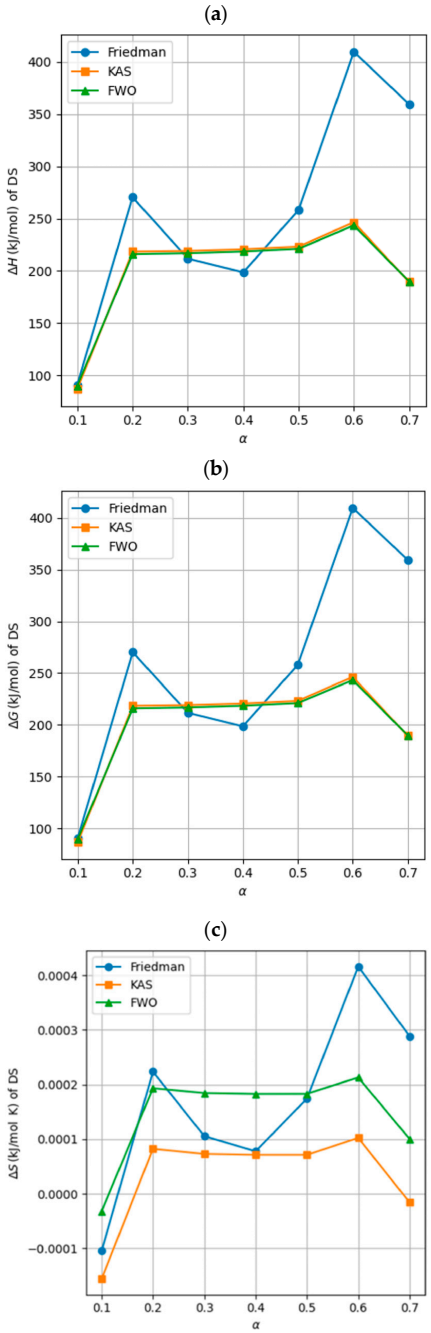

Figure 11. Pure DS thermodynamic parameters (by Friedman, KAS, and FWO models): (**a**) Δ*H*; (**b**) ΔG; (**c**) Δ*S*.

Conversely, the decreasing Δ*S* values at higher conversion rates suggest a shift toward char formation and structural stabilization. Notably, the entropy change further supports the idea of increasing disorder at early stages of decomposition, stabilizing as the process reaches higher conversions, and indicating the complexity of the thermal degradation process in date seeds.

3.3.2. Blended Samples

According to Figure 12, the Friedman model provides consistent thermodynamic values, with the high average enthalpy indicating a significant energy requirement, which is typical for biomass decomposition. The Gibbs free energy follows a similar trend as enthalpy, remaining positive and suggesting a non-spontaneous process that requires

external energy input. The entropy change is modest, reflecting a moderately ordered transition during decomposition. Additionally, the averaged thermodynamic values for Blend 1 are lower than those of the pure samples, supporting the earlier conclusion that the higher proportion of DS in the blend leads to a more energy-efficient pyrolysis process compared to the individual components. This further confirms that the addition of DS reduces the overall energy demand.

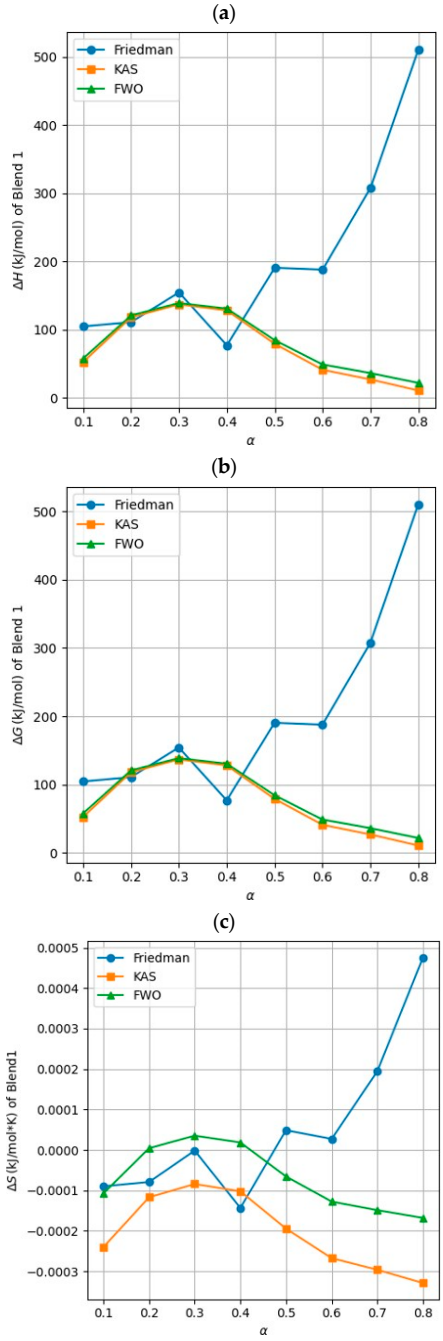

Figure 12. Blends 1 thermodynamic parameters (by Friedman, KAS, and FWO models): (**a**) ΔH; (**b**) ΔG; (**c**) ΔS.

The decomposition of Blend 2 (50% DS, 50% SCG) involves complex thermodynamic phases, and the enthalpy and Gibbs free energy follow the same trend as the DS sample and Blend 1 in the initial and mid stages (Figure 13). The late stages (α = 0.7) show a decline in energy requirements and a more stable entropy profile, which may reflect

char formation and the stabilization of the remaining biomass. The KAS model, with its smoother trends, seems to offer the most reliable representation of thermal behaviour for this blend, while the Friedman model's sharp fluctuations may be attributed to its sensitivity to experimental conditions.

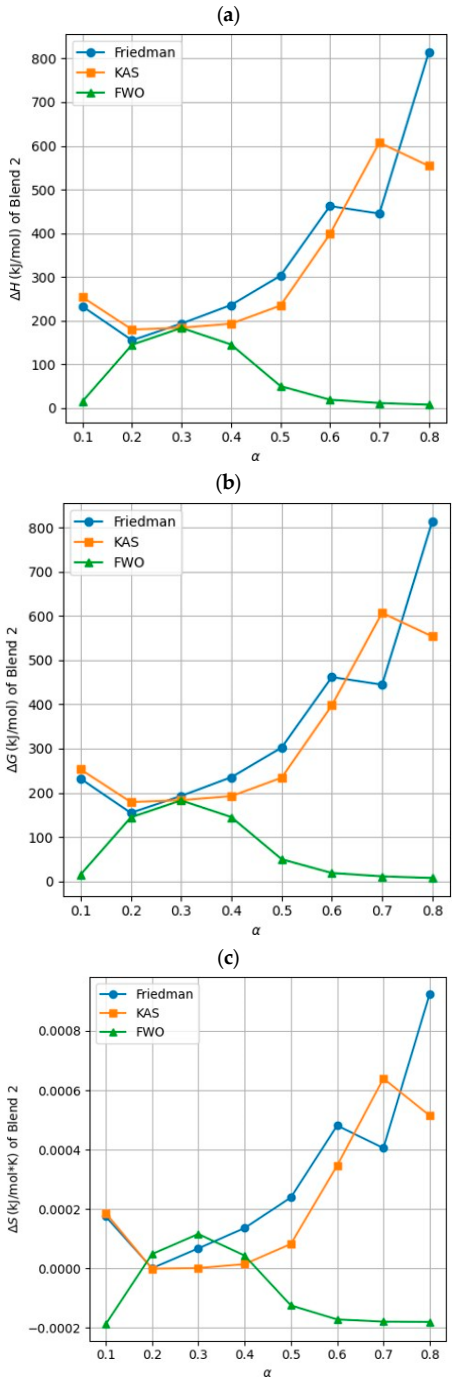

Figure 13. Blends 2 thermodynamic parameters (by Friedman, KAS, and FWO models): (**a**) ΔH; (**b**) ΔG; (**c**) ΔS.

The decomposition of Blend 3 (25% DS, 75% SCG) exhibits distinct thermodynamic phases, similar to the other biomass blends (Figure 14). At the late stage (α = 0.7), energy requirements and entropy decline. The KAS model, with its stable thermodynamic parameters, proves to be the most robust method for analyzing both kinetic and thermodynamic behaviour during Blend 3 decomposition, while the Friedman model, although providing

more detailed insights, is highly sensitive to experimental variations. Overall, the thermodynamic parameters indicate that Blend 3 requires considerable external energy for pyrolysis, with a higher energy demand than all of the other samples, reflecting the higher proportion of SCG in this blend.

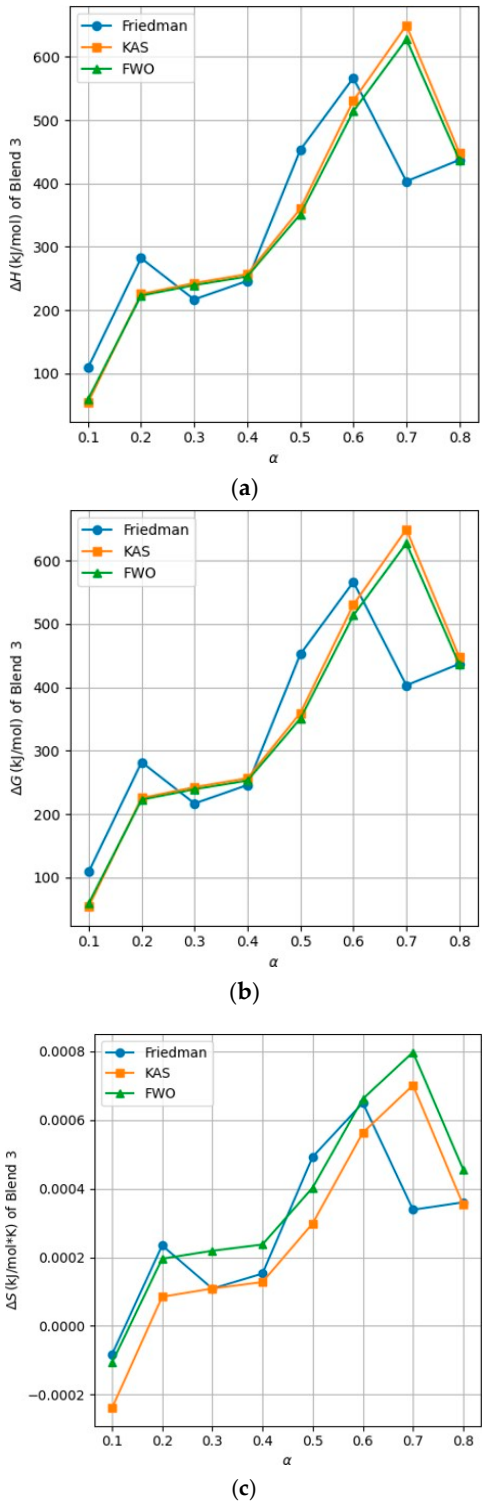

Figure 14. Blends 3 thermodynamic parameters (by Friedman, KAS, and FWO models): (**a**) ΔH; (**b**) ΔG; (**c**) ΔS.

3.4. Pyrolysis Product Analysis

3.4.1. Solid Yields (Char and Volatiles)

The pyrolysis reaction was performed on the five different samples, as given above. The results for each test are summarized in Table 11. The η values represent the char percentage yielded after the pyrolysis process, and the VM% is the volatile matter yielded by each sample and calculated according to Equation (1):

$$VM\% = 100\% - \eta(\%) \quad (1)$$

Table 11. Char yield and volatile matter percentage for different biomass samples.

Sample	VM Yield %	Char Yield (η) %
100% DS	72.26	27.74
100% SCG	72.16	27.84
75% DS–25% SCG	70.69	29.04
50% DS–50% SCG	71.59	28.41
25% DS–75% SCG	73.61	26.39

The volatile matter (VM) and char yields of pure DS, pure SCG, and their blends are summarized in Table 11. The VM yields of the two pure feedstocks are remarkably similar 72.26 wt% for DS and 72.16 wt% for SCG, indicating a comparable devolatilization potential for both agro-industrial residues under the applied pyrolysis conditions, consistent with their similar proximate analysis profiles.

The blending ratio exerts a non-monotonic influence on the VM yield. Blend 1 (75% DS/25% SCG) exhibits the lowest VM yield among all samples (70.69 wt%), accompanied by the highest char yield (29.04 wt%), suggesting that the specific interaction between DS and SCG at this blending ratio promotes char formation at the expense of volatile release. This behaviour may reflect a negative synergistic effect on devolatilization in DS-dominant blends, wherein the dense lignocellulosic matrix of DS inhibits the full volatilization of SCG-derived intermediates, favouring secondary char-forming condensation reactions.

Blend 2 (50% DS/50% SCG) shows an intermediate VM yield of 71.59 wt% with a char yield of 28.41 wt%, representing a partial recovery toward the pure feedstock values as the proportion of each component reaches equilibrium. Blend 3 (25% DS/75% SCG), however, exhibits the highest VM yield of all samples including the pure feedstocks (73.61 wt%), with the correspondingly lowest char yield (26.39 wt%). This enhancement in volatile matter release beyond the individual feedstock values constitutes evidence of a positive synergistic effect on devolatilization in SCG-dominant blends. Positive synergistic effects on volatile matter yield in co-pyrolysis have been attributed to the hydrogen-rich volatile intermediates generated from lipid-rich feedstocks, which can stabilize and promote the release of oxygenated volatiles from the co-feedstock through hydrogen radical transfer mechanisms, thereby suppressing char-forming repolymerization reactions.

These results collectively suggest that the blending ratio constitutes a critical parameter for controlling the distribution between volatile and solid pyrolysis products in DS/SCG co-pyrolysis systems, with SCG-dominant compositions (Blend 3) offering the most favourable profile for maximizing volatile and therefore gas and bio-oil production.

Pyrolysis involves heating a sample under controlled conditions, breaking it into smaller fragments, which are then analyzed using micro-GC to identify and quantify the resulting components. In our specific case, the gases were collected in a Tedlar bag after pyrolysis of biomass at a heating rate of 10 °C/min and a final temperature of 600 °C and subsequently injected into the micro-GC for analysis. In this study, the Py-micro-GC analysis provided data on various gas components. The measured gases included hydrogen

(H_2), methane (CH_4), nitrogen (N_2), acetylene (C_2H_2), oxygen (O_2), carbon monoxide (CO), and carbon dioxide (CO_2). Ethane (C_2H_6) was also quantified to further characterize the pyrolysis gas.

3.4.2. Incondensable Gas (Micro-GC)

Micro-GC analysis of the non-condensable gases produced during pyrolysis of DS and SCG at 600 °C (heating rate 10 °C/min) reveals significant compositional differences that reflect the distinct biochemical nature of each feedstock (Table 12). All concentrations are expressed in weight percent (wt%).

Table 12. Gas analysis for DS and SCG samples pyrolysis.

Component	Concentration (wt%)	
	DS	SCG
H_2	15.96	56.98
CH_4	43.97	13.30
CO	21.63	9.00
CO_2	12.94	7.65
C_2H_2 + C_2H_4	2.13	5.67
C_2H_6	3.37	7.40

The gas fraction from DS is dominated by methane (CH_4: 43.97 wt%), followed by carbon monoxide (CO: 21.63 wt%), hydrogen (H_2: 15.96 wt%), and carbon dioxide (CO_2: 12.94 wt%). In contrast, SCG produces a gas composition strongly oriented toward hydrogen (H_2: 56.98 wt%), with significantly lower concentrations of CH_4 (13.30 wt%), CO (9.00 wt%), and CO_2 (7.65 wt%). This fundamental contrast in gas selectivity can be directly traced to the distinct macromolecular compositions of the two feedstocks.

A dense lignocellulosic matrix rich in cellulose, hemicellulose, and lignin characterize DS. SCG, by contrast, is a lipid- and nitrogen-rich biomass whose high volatile matter content and aliphatic hydrocarbon chains undergo extensive thermal dehydrogenation at 600 °C. The high heating value of SCG (21.4 MJ/kg) reflects its rich extractives content, and the lipid fraction plays a central role in driving the thermochemical conversion pathways, generating aliphatic intermediates that are subsequently cracked into hydrogen-rich gaseous products. The thermal degradation of carbonyl and carboxyl groups in the three lignocellulosic components is thought to produce CO_2 and CO at lower temperatures, while at higher temperatures these are consumed or converted through secondary reactions.

From the perspective of hydrogen production through thermochemical valorization of agro-industrial wastes, the results clearly identify SCG as the superior feedstock, yielding 56.98 wt% H_2, nearly 3.6 times the H_2 content obtained from DS pyrolysis (15.96 wt%). SCG is recognized as a promising lignocellulosic material rich in carbohydrates, proteins, and polyphenols, offering strong valorization potential for biofuel production including H_2, and its thermochemical conversion at elevated temperatures yields significantly hydrogen-enriched gaseous fractions. However, DS—despite its lower H_2 yield—generates a gas fraction with a high combined calorific value, owing to the co-production of CH_4 (43.97 wt%) and CO (21.63 wt%), which together constitute a high-energy-density syngas suitable for energy recovery applications such as combined heat and power generation or gas-to-liquid conversion.

In conclusion, both DS and SCG demonstrate distinct but complementary thermochemical profiles that position them as viable feedstocks for different hydrogen production and energy recovery strategies within an agro-industrial waste biorefinery framework. SCG is favoured for direct hydrogen-oriented pyrolysis applications, while DS is better suited for syngas production or methane-rich gas recovery processes.

The micro-GC analysis of the non-condensable gas fractions produced during co-pyrolysis of DS/SCG blends at 600 °C (10 °C/min) reveals a systematic and highly informative evolution of gas composition as a function of the blending ratio (Table 13). All concentrations are expressed in weight percent (wt%).

Table 13. Gas analysis for Blends 1, 2 and 3.

Component	Concentration (wt%)		
	Blend 1 *	**Blend 2 ***	**Blend 3 ***
H_2	38.113	38.63	41.13
CH_4	18.679	19.17	19.06
CO	16.981	15.02	18.35
CO_2	15.472	12.16	7.55
$C_2H_2 + C_2H_4$	5.094	6.58	6.59
C_2H_6	5.660	8.44	7.31

* Blend 1: 75%DS25%SCG, Blend 2: 50%DS50%SCG, Blend 3: 25%DS 75%SCG.

Comparing the blend gas compositions with those of the individual feedstocks reveals that co-pyrolysis systematically enhances the production of energetically valuable species (H_2, CH_4, and C_2H_x), while generating intermediate CO and CO_2 profiles positioned between the two parent feedstocks. The combined H_2 + CH_4 content across the blends reaches 55.09 wt% (Blend 1), 57.80 wt% (Blend 2), and 60.19 wt% (Blend 3), values that substantially exceed any weighted average of the individual pyrolysis results and confirm the net positive energetic benefit of the co-pyrolysis strategy. Co-pyrolysis of biomass blends has been identified as a promising strategy for producing higher yields of syngas and value-added gaseous products compared to using single feedstocks.

From a hydrogen production perspective, Blend 3 (25%DS/75%SCG) delivers the highest H_2 content (41.13 wt%) and the lowest CO_2 fraction (7.55 wt%), making it the most favourable formulation for direct hydrogen-oriented applications. Blend 2 (50%DS/50%SCG) represents an attractive compromise, offering a high combined H_2 + CH_4 yield (57.80 wt%) with a balanced CO/CO_2 profile suited for syngas generation or combined heat and power applications. Reforming the volatile fraction of biomass pyrolysis products including H_2, CH_4 and light C_2 hydrocarbons represents a viable and underexplored method to further enhance hydrogen yield from agro-industrial biomass wastes, with the co-produced CH_4 and C_2 species serving as H_2 precursors for downstream catalytic steam reforming. In this context, the gas fractions from all three DS/SCG blends constitute promising feedstocks for integrated pyrolysis-reforming processes targeting green hydrogen production from agro-industrial waste valorization.

The results of this study's experimental sections may serve as a helpful manual for producing biogas and biochar on an industrial scale from various agricultural wastes. The findings of the study provide useful guidance for the industrial-scale production of H2 and biochar from these feedstocks, which can be used as a catalytic support, water pollutant adsorbent, and gas adsorbent in various chemical production, purification, and storage processes. The synthesis of biohydrogen from waste lignocellulosic biomass accomplishes the dual purpose of converting waste into valuable products and reduces waste disposal issues. Co-pyrolysis has been identified as a promising method for improving the performance of the biomass pyrolysis process through synergistic interactions.

3.5. Prediction Results

This subsection presents the obtained results of the LSTM model with two different datasets for pure biomasses and their blends. Model 1, which only uses basic features (temperature, heating rate, and blend ratios), achieving comparable or superior accuracy

to ANN models from the literature. For instance, Tariq et al. [38] achieved R^2 values of 0.975–0.996 for TGA predictions of biomass blends, while Model 1 in this study yielded similar R^2 values (0.9658–0.9958) (Table 13), despite using a smaller, less diverse dataset. Another relevant study by Yildiz et al. [39] reported an exceptional R^2 of 0.9995 for predicting TGA curves of hazelnut husk and lignite coal blends at varying heating rates. Their results slightly outperform Model 1 (Table 13), likely due to their dataset's greater diversity in heating rates and blend ratios. Similarly, Bi et al. [40] achieved an R^2 of 0.99972 by incorporating a wide range of blend ratios and heating rates in their ANN model. These findings emphasize the importance of dataset diversification to enhance model generalization.

Model 1's limitations remain, particularly with predicting profiles for higher heating rates and unseen blend ratios, underscoring the need for more diverse training data (Figures 15 and 16). Despite these differences, the LSTM models exhibited robust performance, as demonstrated by the achieved loss metrics (Table 14).

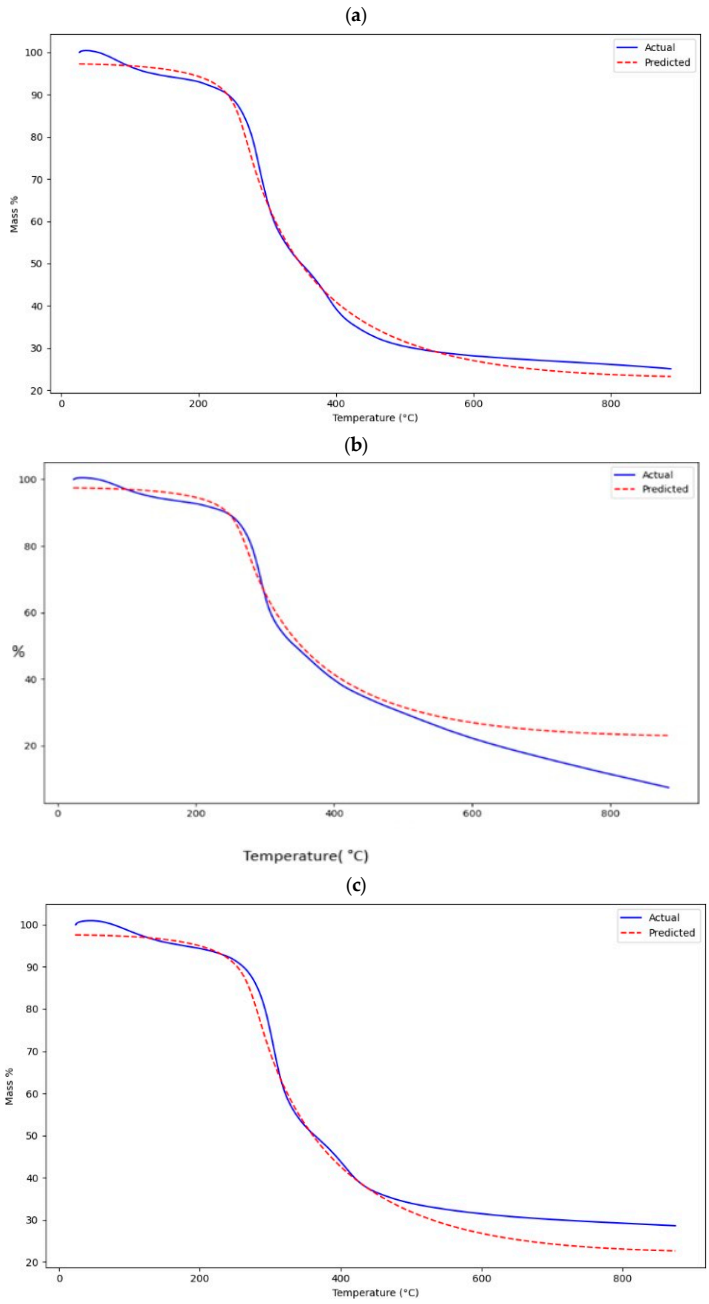

Figure 15. Model 1's prediction of Blend 1's TGA data: (**a**) 10 °C/min; (**b**) 15 °C/min; (**c**) 25 °C/min.

(**a**)

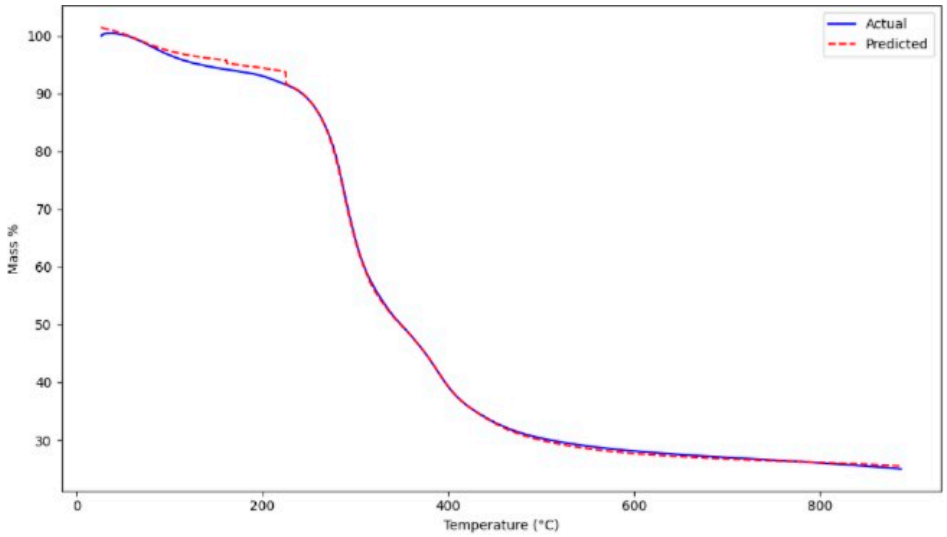

(**b**)

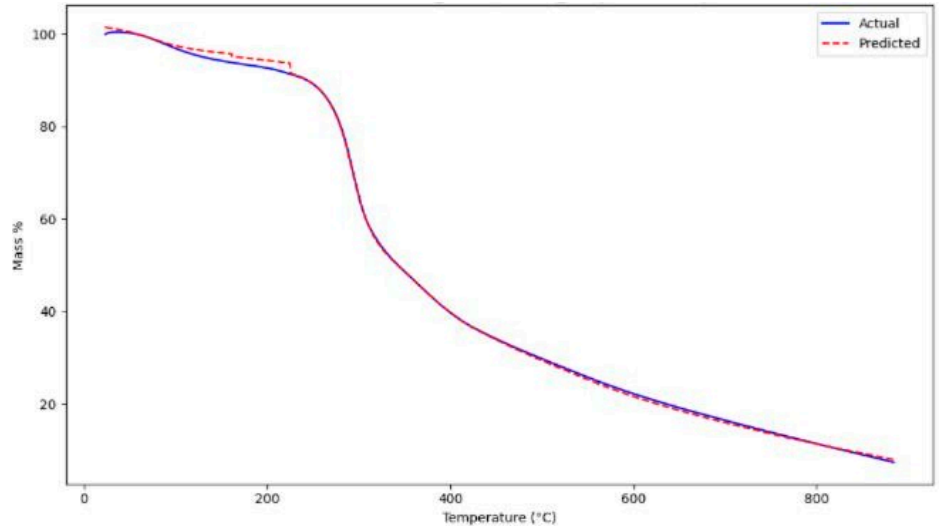

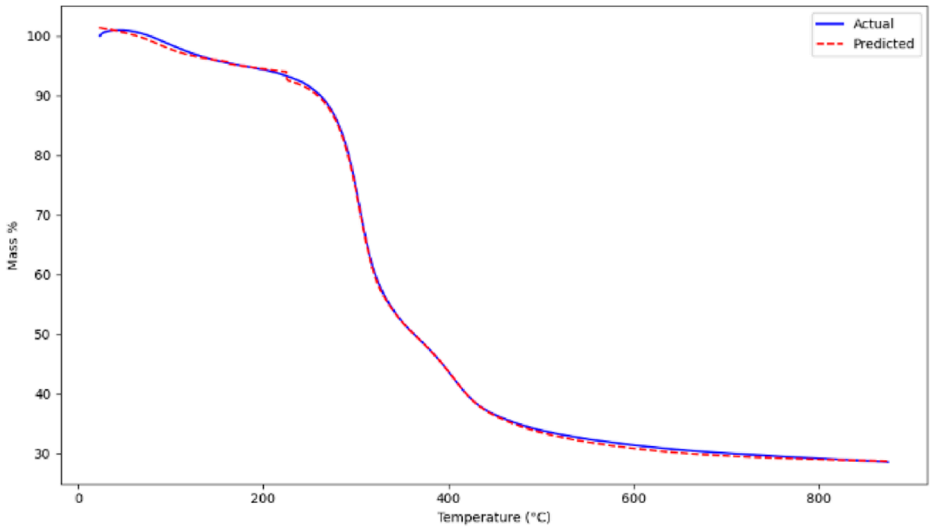

(**c**)

Figure 16. Model 2's prediction of blend 1's TGA data: (**a**) 10 °C/min; (**b**) 15 °C/min; (**c**) 25 °C/min.

Table 14. Comparison of error metrics: Model 1 vs. Model2.

Error Metrics	Model 1 *			Model 2 *		
	10 °C/min	15 °C/min	25 °C/min	10 °C/min	15 °C/min	25 °C/min
R^2	0.9958	0.9658	0.9830	0.9996	0.9996	0.9998
MSE	3.6557	39.3286	14.9231	0.3586	0.4637	0.1809
MAE	1.6525	4.6805	3.1518	0.4206	0.4828	0.3509
RMSE	1.9120	6.2713	3.8630	0.5988	0.6809	0.4254

* Model 1: trained on temperature, heating rates and ratios. * Model 2: trained on lignocellulosic composition, temperature, heating rates and ratio features.

Incorporating lignocellulosic composition as additional features in Model 2 further enhanced prediction accuracy, especially for unseen heating rates like 25 °C/min, as shown in Figure 16a–c. This improvement is evident in the significantly lower error metrics (MSE and MAE) and higher R^2 values compared to Model 1 (Table 13).

Model 1 (Figure 15) faced challenges in accurately predicting TGA profiles for unseen heating rates and blend ratios. For instance, the model's performance declined at higher heating rates like 15 °C/min and 25 °C/min (Table 13), which were not included in the training data. This limitation can be attributed to the lack of data diversity, as seen in previous studies [38–41], where diversified datasets resulted in higher predictive accuracy. Contrarily, Model 2 (Figure 16) addressed this limitation by incorporating lignocellulosic composition features, which provided a deeper understanding of biomass thermal decomposition. As shown in Table 13, this improvement led to significantly lower error metrics (MSE and MAE) and higher R^2 values. However, the results indicate that further enhancements, such as increasing dataset diversity, could further boost model performance.

4. Conclusions and Perspectives

This research emphasizes the importance of shifting from fossil fuel-based "Gray hydrogen" to renewable "green hydrogen" using underutilized biomass resources and machine learning (specifically deep learning) applications. The study explored the thermal, kinetic, and thermodynamic behaviours of spent coffee grounds (SCGs) and date seeds (DSs), and their blends for hydrogen production through pyrolysis process.

The results demonstrate that DS, SCG, and their blends, hold significant promise for bioenergy production. Blend 3 (75% SCG–25% DS) emerged as the most favourable for hydrogen production, with highest volatile matter release. However, it requires highest energy input. Blend 1 (75% DS–25% SCG) demonstrated superior energy efficiency with lowest energy demand. Building on these experimental findings, the study explores the LSTM modelling approach to predict TGA mass loss patterns, significantly outperforming traditional methods, with exceptional accuracy ($R^2 > 0.999$), while considering the lignocellulosic composition of pure biomasses and their blends. These findings demonstrate that combining experimental and predictive approaches can promote the bioenergy production while reducing reliance on time- intensive TGA experiments and pyrolysis reactors.

As perspectives, future work will focus on expanding the diversity of the dataset to other biomasses, and to predict blend behaviour. An attempt to eliminate the need for blend-specific training data is envisaged. Additional efforts will enhance dataset diversity in blend ratios and applied heating rates in order to improve model generalization.

Author Contributions: Conceptualization, S.K., A.S. and Z.M.; methodology, S.K., A.S. and Z.M.; software; validation, S.K., A.S. and M.A.; formal analysis, O.B.; investigation, O.B.; resources, K.C. and Z.M.; data curation, O.B.; writing-original draft preparation, Z.M.; writing-review and editing, A.S., M.A. and Z.M.; visualization, supervision, A.S.; project administration, A.S.; funding acquisition, K.C. All authors have read and agreed to the published version of the manuscript.

Funding: This research received no external funding.

Data Availability Statement: Data will be made available on request.

Conflicts of Interest: The authors declare no conflict of interest.

References

1. Diez, J.R.; Tomé-Torquemada, S.; Vicente, A.; Reyes, J.; Orcajo, G.A. Decarbonization pathways, strategies, and use cases to achieve net-zero CO_2 emissions in the steelmaking industry. *Energies* **2023**, *16*, 7360. [CrossRef]
2. Intergovernmental Panel on Climate Change. Climate change 2007: The physical science basis. *Agenda* **2007**, *6*, 333.
3. IRENA. *Hydrogen: A Renewable Energy Perspective*; IRENA: Abu Dhabi, United Arab Emirates, 2019.
4. Susanto, F.L.; Maulani, A.; Nuri, S.N. Implementation of Big Data Analytics and its Challenges in Digital Transformation Era: A Literature Review. *Int. J. Inform. Inf. Syst.* **2024**, *7*, 90–99. [CrossRef]
5. Mayol, A.P.; Maningo, J.M.Z.; Chua-Unsu, A.G.A.Y.; Felix, C.B.; Rico, P.I.; Chua, G.S.; Manalili, E.V.; Fernandez, D.D.; Cuello, J.L.; Bandala, A.A.; et al. Application of Artificial Neural Networks in prediction of pyrolysis behavior for algal mat (LABLAB) biomass. In *2018 IEEE 10th International Conference on Humanoid, Nanotechnology, Information Technology, Communication and Control, Environment and Management (HNICEM)*; IEEE: New York, NY, USA, 2018; pp. 1–5.
6. Mutlu, A.Y.; Yucel, O. An artificial intelligence based approach to predicting syngas composition for downdraft biomass gasification. *Energy* **2018**, *165*, 895–901. [CrossRef]
7. Aghbashlo, M.; Tabatabaei, M.; Nadian, M.H.; Davoodnia, V.; Soltanian, S. Prognostication of lignocellulosic biomass pyrolysis behavior using ANFIS model tuned by PSO algorithm. *Fuel* **2019**, *253*, 189–198. [CrossRef]
8. Zhu, X.; Li, Y.; Wang, X. Machine learning prediction of biochar yield and carbon contents in biochar based on biomass characteristics and pyrolysis conditions. *Bioresour. Technol.* **2019**, *288*, 121527. [CrossRef]
9. Cheng, F.; Luo, H.; Colosi, L.M. Slow pyrolysis as a platform for negative emissions technology: An integration of machine learning models, life cycle assessment, and economic analysis. *Energy Convers. Manag.* **2020**, *223*, 113258. [CrossRef]
10. Farah, J.S.; Cavalcanti, R.N.; Guimarães, J.T.; Balthazar, C.F.; Coimbra, P.T.; Pimentel, T.C.; Esmerino, E.A.; Duarte, M.C.K.; Freitas, M.Q.; Granato, D.; et al. Differential scanning calorimetry coupled with machine learning technique: An effective approach to determine the milk authenticity. *Food Control* **2021**, *121*, 107585. [CrossRef]
11. Muravyev, N.V.; Luciano, G.; Ornaghi, H.L., Jr.; Svoboda, R.; Vyazovkin, S. Artificial neural networks for pyrolysis, thermal analysis, and thermokinetic studies: The status quo. *Molecules* **2021**, *26*, 3727. [CrossRef]
12. Balsora, H.K.; Kartik, S.; Joshi, J.B.; Sharma, A.; Chakinala, A.G. Artificial neural network-based models for the prediction of biomass pyrolysis products from preliminary analysis. *Ind. Eng. Chem. Res.* **2023**, *62*, 14311–14319. [CrossRef]
13. Kartal, F.; Özveren, U. Prediction of activation energy for combustion and pyrolysis by means of machine learning. *Therm. Sci. Eng. Prog.* **2022**, *33*, 101346. [CrossRef]
14. Shiri, F.M.; Perumal, T.; Mustapha, N.; Mohamed, R. A comprehensive overview and comparative analysis on deep learning models: CNN, RNN, LSTM, GRU. *arXiv* **2023**, arXiv:2305.17473. [CrossRef]
15. Omar, I.; Khan, M.; Starr, A. Compatibility and challenges in machine learning approach for structural crack assessment. *Struct. Health Monit.* **2022**, *21*, 2481–2502. [CrossRef]
16. El May, Y.; Dorge, S.; Jeguirim, M.; Trouvé, G.; Said, R. Measurement of gaseous and particulate pollutants during combustion of date palm wastes for energy recovery. *Aerosol Air Qual. Res.* **2012**, *12*, 814–825. [CrossRef]
17. Mhemed, H.A.; Largeau, J.-F.; Kordoghli, S.; Gallego, M.M.; Zagrouba, F.; Tazerout, M. Kinetic Study of Lignocellulosic Biomasses Pyrolysis Using Thermogravimetric Analysis. *Int. J. Biomass Renew.* **2020**, *9*, 25. [CrossRef]
18. Khiari, B.; Abed, I.; Jeguirim, M.; Zagrouba, F. Thermal Characterization and Kinetic Study of Palm Trees Wastes During TGA Inert Pyrolysis. Available online: https://www.researchgate.net/profile/Fethi-Zagrouba/publication/234065059_THERMAL_CHARACTERIZATION_AND_KINETIC_STUDY_OF_PALM_TREES_WASTES_DURING_TGA_INERT_PYROLYSIS/links/09e4150ec74739d0c6000000/THERMAL-CHARACTERIZATION-AND-KINETIC-STUDY-OF-PALM-TREES-WASTES-DURING-TGA-INERT-PYROLYSIS.pdf (accessed on 5 February 2026).
19. Nasser, R.A.; Salem, M.Z.M.; Hiziroglu, S.; Al-Mefarrej, H.A.; Mohareb, A.S.; Alam, M.; Aref, I.M. Chemical analysis of different parts of date palm (*Phoenix dactylifera* L.) using ultimate, proximate and thermo-gravimetric techniques for energy production. *Energies* **2016**, *9*, 374. [CrossRef]
20. Abdallah, A.B.; Trabelsi, A.B.H.; Navarro, M.V.; Veses, A.; García, T.; Mihoubi, D. Pyrolysis of tea and coffee wastes: Effect of physicochemical properties on kinetic and thermodynamic characteristics. *J. Therm. Anal. Calorim.* **2023**, *148*, 2501–2515. [CrossRef] [PubMed]
21. Fassatoui, E.; Jeguirim, M.; Zorpas, A.A.; Khiari, B. Experimental and feasibility study of bio-waste valorization through pyrolysis for energy and materials production in the concept of circular economy. *Process Saf. Environ. Prot.* **2024**, *187*, 279–291.

22. Fermoso, J.; Mašek, O. Thermochemical decomposition of coffee ground residues by TG-MS: A kinetic study. *J. Anal. Appl. Pyrolysis* **2018**, *130*, 358–367. [CrossRef]
23. Franca, A.S.; Oliveira, L.S. Potential uses of spent coffee grounds in the food industry. *Foods* **2022**, *11*, 2064. [CrossRef]
24. Narnaware, S.L.; Panwar, N.L. Pyrolysis kinetics of lignocellulosic waste biomass (*Cicer arietinum*) using iso-conversional methods. *J. Agric. Eng.* **2022**, *59*, 293–308.
25. Chen, D.; Shuang, E.; Liu, L. Analysis of pyrolysis characteristics and kinetics of sweet sorghum bagasse and cotton stalk. *J. Therm. Anal. Calorim.* **2018**, *131*, 1899–1909. [CrossRef]
26. Bouaziz, F.; Ben Abdeddayem, A.; Koubaa, M.; Barba, F.J.; Ben Jeddou, K.; Kacem, I.; Ghorbel, R.E.; Chaabouni, S.E. Bioethanol production from date seed cellulosic fraction using *Saccharomyces cerevisiae*. *Separations* **2020**, *7*, 67. [CrossRef]
27. Fersi, M.; Mbarki, K.; Gargouri, K.; Mechichi, T.; Hachicha, R. Assessment of organic matter biodegradation and physico-chemical parameters variation during co-composting of lignocellulosic wastes with *Trametes trogii* inoculation. *Environ. Eng. Res.* **2019**, *24*, 670–679. [CrossRef]
28. Sorek, N.; Yeats, T.H.; Szemenyei, H.; Youngs, H.; Somerville, C.R. The implications of lignocellulosic biomass chemical composition for the production of advanced biofuels. *Bioscience* **2014**, *64*, 192–201. [CrossRef]
29. Carrier, M.; Joubert, J.-E.; Danje, S.; Hugo, T.; Görgens, J.; Knoetze, J.H. Impact of the lignocellulosic material on fast pyrolysis yields and product quality. *Bioresour. Technol.* **2013**, *150*, 129–138. [CrossRef]
30. Fisher, T.; Hajaligol, M.; Waymack, B.; Kellogg, D. Pyrolysis behavior and kinetics of biomass derived materials. *J. Anal. Appl. Pyrolysis* **2002**, *62*, 331–349. [CrossRef]
31. Fadhil, A.B.; Alhayali, M.A.; Saeed, L.I. Date (*Phoenix dactylifera* L.) palm stones as a potential new feedstock for liquid bio-fuels production. *Fuel* **2017**, *210*, 165–176. [CrossRef]
32. Kok, M.V.; Ozgur, E. Characterization of lignocellulose biomass and model compounds by thermogravimetry. *Energy Sources Part A Recovery Util. Environ. Eff.* **2017**, *39*, 134–139.
33. Dash, M.; Dasu, V.V.; Mohanty, K. Non-isothermal kinetic study of three lignocellulosic biomass using model-free methods. *J. Renew. Sustain. Energy* **2013**, *5*, 063101. [CrossRef]
34. Alsulami, R.A.; El-Sayed, S.A.; Eltaher, M.A.; Mohammad, A.; Almitani, K.H.; Mostafa, M.E. Pyrolysis kinetics and thermal degradation characteristics of coffee, date seed, and prickly pear wastes and their blends. *Renew. Energy* **2023**, *216*, 119039. [CrossRef]
35. Bartolucci, L.; Cordiner, S.; Di Carlo, A.; Gallifuoco, A.; Mele, P.; Mulone, V. Platform chemicals recovery from spent coffee grounds aqueous-phase pyrolysis oil. *Renew. Energy* **2024**, *220*, 119630. [CrossRef]
36. Gupta, G.K.; Mondal, M.K. Kinetics and thermodynamic analysis of maize cob pyrolysis for its bioenergy potential using thermogravimetric analyzer. *J. Therm. Anal. Calorim.* **2019**, *137*, 1431–1441. [CrossRef]
37. Annapureddy, P.K.R.; Ranjan, A.; Kishore, N. Kinetics, reaction models, and thermodynamic feasibility of non-isothermal catalytic pyrolysis of *Erythrina indica*. *J. Renew. Sustain. Energy* **2025**, *17*, 023102. [CrossRef]
38. Tariq, R.; Zaifullizan, Y.M.; Salema, A.A.; Abdulatif, A.; Ken, L.S. Co-pyrolysis and co-combustion of orange peel and biomass blends: Kinetics, thermodynamic, and ANN application. *Renew. Energy* **2022**, *198*, 399–414. [CrossRef]
39. Yıldız, Z.; Uzun, H.; Ceylan, S.; Topcu, Y. Application of artificial neural networks to co-combustion of hazelnut husk–lignite coal blends. *Bioresour. Technol.* **2016**, *200*, 42–47. [CrossRef] [PubMed]
40. Bi, H.; Wang, C.; Jiang, X.; Jiang, C.; Bao, L.; Lin, Q. Thermodynamics, kinetics, gas emissions and artificial neural network modeling of co-pyrolysis of sewage sludge and peanut shell. *Fuel* **2021**, *284*, 118988. [CrossRef]
41. Kordoghli, S.; Settar, A.; Belaati, O.; Alkhatib, M.; Chetehouna, K.; Mansouri, Z. Hydrogen production from blended waste biomass: Pyrolysis, thermodynamic-kinetic analysis and AI-based modelling. *arXiv* **2025**, arXiv:2510.15960. [CrossRef]